Malaria Parasite Classification from RBC Smears Using Lightweight Parallel Depthwise Separable CNN and Ridge Regression ELM by Integrating SHAP Techniques

Md. Faysal Ahamed
Rajshahi University of Engineering and Technology
Md. Nahiduzzaman
Rajshahi University of Engineering and Technology
Mohamed Arselene Ayari
Qatar University
Amit Khandakar (amitk@qu.edu.qa)
Qatar University
S. M. Riazul Islam
University of Aberdeen

Research Article

Keywords: Convolutional Neural Networks (CNN), Ridge Regression Extreme Learning Machines (RELM), Contrast-limited adaptive histogram equalization (CLAHE), Dilation, Malaria Parasites, Classification and Shapley Additive Explanations (SHAP).

Posted Date: September 29th, 2023

DOI: https://doi.org/10.21203/rs.3.rs-3358084/v1

Additional Declarations: No competing interests reported.

Malaria Parasite Classification from RBC Smears Using Lightweight Parallel Depthwise Separable CNN and Ridge Regression ELM by Integrating SHAP Techniques

Md. Faysal Ahamed[1], Md. Nahiduzzaman[2], Mohamed Arselene Ayari[3], Amith Khandakar[4, *], S. M. Riazul Islam[5, *]

[1]Department of Computer Science & Engineering, Rajshahi University of Engineering & Technology, Rajshahi-6204, Bangladesh.

[2]Department of Electrical & Computer Engineering, Rajshahi University of Engineering & Technology, Rajshahi-6204, Bangladesh.

[4]Department of Civil and Environmental Engineering, Qatar University, Doha 2713, Qatar.
[4]Department of Electrical Engineering, Qatar University, Doha 2713, Qatar.

[5]Department of Computing Science, University of Aberdeen, Aberdeen AB24 3FX, UK.

Correspondence

Amith Khandakar (amitk@qu.edu.qa), S. M. Riazul Islam (riazul.islam@abdn.ac.uk)

Abstract

Malaria is a significant health concern worldwide, and early detection and accurate classification are essential for better treatment. This study proposes a new method that combines a lightweight parallel depth-wise separable convolutional neural network (LPDCNN) with a hybrid ridge regression extreme learning machine (RELM) to classify images of infected and uninfected patients' red blood cells (RBCs). We include a hybrid pre-processing step that uses contrast-limited adaptive histogram equalization (CLAHE) and Dilation operation to enhance image quality, reduce cell noise, and improve visual acuity. The LPDCNN extracts discriminative features efficiently with only 0.36 million parameters and 8 layers, minimizing computational complexity. The hybrid RELM model improves classification performance and replaces the traditional pseudoinverse of the ELM approach. Rigorous five-fold cross-validation (CV) for binary class classifications shows that the framework has impressive average precision, recall, f1, accuracy, and AUC scores of 99.86±0.08%, 99.88±0.084%, 99.84±0.089%, 99.85±0.071%, and 99.96±0.037%, respectively, surpassing state-of-the-art (SOTA) models. The proposed framework is exceptionally efficient, with an average training and testing time of 0.1376 and 0.00255 seconds, respectively. Additionally, the framework is integrated SHAP (Shapley Additive Explanations) to enhance interpretability, providing valuable insights into decision-making and instilling confidence in malaria diagnosis for real-world applications. This comprehensive approach holds promise in improving malaria diagnosis and patient outcomes worldwide.

Keywords
Convolutional Neural Networks (CNN), Ridge Regression Extreme Learning Machines (RELM), Contrast-limited adaptive histogram equalization (CLAHE), Dilation, Malaria Parasites, Classification and Shapley Additive Explanations (SHAP).

1. Introduction

According to the World Health Organization (WHO), in 2015, 300 to 500 million people were infected with malaria parasites, resulting in 438,000 deaths. Shockingly, in 2017, this number increased to 620,000 [1]. The transmission of the malaria virus is significantly influenced by meteorological conditions that enable mosquitoes to survive for more extended periods. Regions with elevated environmental temperatures, especially after rainfall, such as Africa, are the most affected by the disease [2]. Other humid regions like Asia and Latin America also serve as breeding grounds for the parasite. The female anopheles' mosquito, which carries the malaria-causing parasites, is responsible for transmitting the illness to humans. Out of the 400 different species of anopheles mosquitoes, only 30 are the primary hosts for the parasites [3]**.** Malaria is a disease that spreads through the bite of a female Anopheles mosquito that has previously fed on an infected human. The Anopheles mosquito goes through four stages of life: egg, larva, pupa, and adult [4]. These mosquitoes need to consume human blood to mature their eggs, which is when malaria transmission can occur. Plasmodium parasites can cause malaria: Plasmodium Falciparum, Plasmodium Vivax, Plasmodium Ovale, Plasmodium Malariae, and Plasmodium Knowlesi. Plasmodium Falciparum and Plasmodium Vivax are the two most dangerous types. After a mosquito bite, it can take anywhere from 10 to 15 days, or even longer, for symptoms to appear. Symptoms include fever, chills, nausea, and vomiting, which occur when the parasite infects and reduces the number of red blood cells. It is crucial to diagnose malaria quickly, as it can progress rapidly and become fatal [2-4].

Malaria can be transmitted in hot and humid regions near water sources [6]. The preferred method for diagnosing the disease is thin-layer microscopy, but it can be time-consuming since at least 5,000 RBC cells need to be manually identified. An alternative method is antigen screening, which is faster but has a higher chance of errors and can be costly. Patients in developing countries often lack access to rapid diagnostic tests and financial support, so it is crucial to develop an efficient and affordable system for malaria diagnosis. Therefore, it is necessary to develop an automated computer-aided diagnostic (CAD) system that can detect the presence of malaria parasites (MPs) at the earliest stage without requiring the involvement of medical professionals [7–10].

Medical research has tended to prioritize binary classification studies, such as distinguishing between Machine Learning (ML) [11-15] and Deep Learning (DL) [16-30] architecture, without fully exploring the complex nuances of MPs.

In their work, Alharbi et al. [11] utilized a convolutional approach coupled with a traditional machine-learning method to classify MPs in blood samples. They trained the model using a total of 13,750 parasitized samples, along with a specific number of uninfected samples. The results showed that support vector machine (SVM) achieved a 94% accuracy rate, XG-Boost achieved 90% accuracy, and the neural network achieved 80% accuracy. When the CNN model was applied

to the dataset, 97% accuracy was achieved, and SVM performed better than the other ML models. Researchers Das et al. [12] created a computer-assisted model for classifying MPs using microscopic images of peripheral blood smears. These images were collected and corrected for noise reduction using strain slides. The team used encrypted segmentation to group similar features into clusters, which improved the accuracy of the final classification results. The samples they collected contained two parasites, P. Vivax, and P. Falciparum. They used a cluster with SVM and Bayesian networks to differentiate between the features, with the Bayesian network achieved an 85% accuracy rate and SVM achieved 83.5%. In their research, Yunda et al. [13] utilized a wavelet-based technique for feature extraction. To simplify the model, they employed morphological image processing for image analysis. By applying Principal Component Analysis (PCA) to reduce the number of susceptible features, they achieved a 77.19% favorable rate in actual results. The thin blood film method is utilized in the clinical sector to segment the malaria parasite manually. Purnama et al. [14] conducted a study that employed techniques such as HSV histogram, hue channel shifting, and genetic programming-based classification. Their findings showed they could accurately identify 95.49% parasites and 95.58% non-parasites from 180 samples. Rosado et al. [15] utilized an automated method to detect thin blood smears on mobile devices. They employed the Traditional SVM classifier on 314 featured images as candidate samples, achieving a specificity of 93.8% and a sensitivity of 80.5%. In addition, White Blood Cell (WBC) displayed exemplary sensitivity and specificity scores of 98.2% and 93.8%, respectively, on those samples.

DL-based models for detecting malaria are more efficient for feature extraction than ML approaches. A deep network is presented by Bibin et al. [16] , where they utilized 4,100 samples for the training set, and after training, they achieved 95.92% specificity, 97.60% sensitivity, and 89.66% F-score.

A CNN model was presented by Rajaraman et al. [17] to extract features from 27,558 samples and detect the MP from RBC segmented images. Their analysis showed an accuracy rate of 92.7%. To detect the MP, Sriporn et al. [18] used six existing models, including Xception [19], Inception-V3 [20]**,** ResNet-50 [21]**,** VGG-16 [22], and AlexNet [23]**.** They employed a trial-and-error method that tested various model layers, activation functions, and optimization parameters to determine the most significant factor for classifying malaria. The highest accuracy of 99.28% was achieved using 7,000 original samples. This research explored the double hidden layer ELM (DELM) method, developed by Goni et al. [24], which utilized a CNN architecture to extract standard characteristics from malaria samples. The paper also compares the main aspects of conventional ELM and DELM. The researchers tested their approach on 27,558 images from MP, including a modified set with 647 fewer false positives. They trained on both data sets, infected-13,132 and uninfected-13,029, and found that DELM outperformed categorization with an accuracy of 97.79% on the original training set and 99.66% on the modified set. Researcher Khan et al. [25] attempted to classify malaria samples using a regular machine learning classifier. They used a Laplacian filter on the RC images to extract meaningful features. The random forest (RF), SVM, and CNN models were evaluated using in-house datasets, and with only three characteristics, they achieved an 86% recall rate. The CNN and SVM models had 95% and 91.66% accuracies, respectively. In their study, Fuhad et al. [26] explored using CNN for automatic malaria diagnosis

by analyzing red blood cell (RBC) images. They employed various preprocessing techniques, including knowledge distillation and data enrichment. The team utilized SVM and k-nearest neighbors (KNNs) to classify malaria cases and achieved an impressive accuracy rate of 99.23%. Islam et al. [27] introduced a novel multiheaded attention-based transformer model to identify malaria parasites in blood cell images. Test results on the original dataset showed an accuracy of 96.41%, precision of 96.44%, recall of 95.88%, f1-score of 96.44%, and AUC of 99.11%. Using the gradient-weighted class activation map (Grad-CAM) technique, they eliminated the model's primary concerns. By refining hyperparameters, they surpassed SOTA methods for malaria parasite detection. The proposed method worked well in terms of correctly identifying malaria. Mohanty et al. [28] conducted a study on detecting MPs, utilizing the autoencoder (AE) and self-organizing maps (SOM) models. Their findings revealed that the AE model outperformed the SOM model, achieved an impressive accuracy rate of 87.5%. Dong et al. [29] also presented their study on detecting MPs, utilizing three transfer learning (TL) models (LeNet, AlexNet, and GoogLeNet), which demonstrated a higher accuracy rate of 95% compared to SVM's 92%. Furthermore, Anggraini et al. [30] developed a highly accurate CAD system for identifying morphological abnormalities in RBC images. Their system improved image contrast through grayscale preprocessing techniques and accurately distinguished the different components of blood cells using global thresholding methods.

Malaria research often relies on the binary classification method, which separates infected and uninfected cases using typical preprocessing techniques. However, to ensure comprehensive analysis, it is crucial to account for all subcategories of malaria samples collected from red blood cells. Trial and error strategies are necessary with the complexity of sample collection and testing procedures in real-world settings. Unfortunately, there appears to be no previous use of Contrast Limited Adaptive Histogram Equalization (CLAHE) with Dilation, a morphological operation, to optimize data processing to extract Mitochondrial Permeability in cells.

However, there was a significant issue with this study regarding computing requirements. The model needed a lot of parameters and layers, leading to longer processing times, which made it challenging to implement the classification model efficiently. Furthermore, some advanced methods require high-quality images for precise classification, making it challenging for real-world applications, especially those involving embedded systems [14-25]. In order to promote the widespread use of malaria classification models and address associated issues, it is essential to improve existing models by reducing the number of parameters, shortening processing times, and enhancing classification performance. This study highlights these challenges and proposes a novel and effective solution [31,32].

To enhance the contrast of the image, we have employed a combination of hybrid CLAHE and Dilation. Our approach for extracting discriminant features involves the use of two architectures: a parallel normal convolutional neural network (PNCNN) and a lightweight parallel depthwise convolutional neural network (LPDCNN). This model is designed to balance computational resources and accuracy in classification. Additionally, we have developed a hybrid ridge regression extreme learning machine (RELM) that accurately classifies segmented cells. This hybrid model balances performance metrics and computational efficiency, making it suitable for

real-world classification applications where speed and accuracy are paramount. In addition, the study utilizes SHAP (Shapley Additive Explanations) analysis to assure the interpretability and validation of the proposed hybrid LPDCNN-RELM model. This analysis provides insight into the model's decisions regarding regions affected by malaria. Through the use of SHAP analysis, the model's interpretability is improved drastically, and its accurate classification decisions are better understood. The main benefits of this research include:

- A hybrid pre-processing method has been developed to enhance the quality of segmented images of RBCs by reducing noise and improving contrast. This technique has proven to be highly effective in improving the performance of deep learning models across a wide range of datasets.
- In addition, a lightweight parallel depthwise separable CNN (LPDCNN) has been developed to enhance the accuracy of detecting malaria-infected regions while reducing computational costs. By extracting important features from the enhanced images, this model is able to classify them with precision and effectiveness.
- An improved model, called the hybrid ridge regression extreme learning machine (RELM) model, replaces the pseudoinverse approach with ridge regression to overcome the limitations of previous ELM models. This innovative method delivers enhanced accuracy in classification.
- Extensive comparisons with the latest SOTA models demonstrate that the proposed framework outperforms them regarding classification accuracy, model parameters, and classification layer complexity.
- The framework's interpretability is highlighted using SHAP (Shapley Additive Explanations), which offers valuable insights into the model's decision-making process. This greater transparency instills confidence and trust in the framework's practical diagnostic capabilities.

In this research, section 2 presents the proposed methodology, dataset description, image pre-processing, model explanation, and classification metrics with a loss function. In Section 4, comprehensive experimental analyses are presented, accompanied by a thorough discussion and comparisons. Interpretability with SHAP is explained in Section 4, and Section 5 demonstrates the conclusion and summary of this research.

2. Methodology

2.1 Proposed Framework

Figure 1 presents a detailed framework for classifying various categories of malaria detection from RBC images, including normal patient cases. The first step involved collecting a comprehensive dataset of infected and uninfected individuals. A hybrid technique called dilation with CLAHE was used to improve the input quality and image contrast. This process reduced image noise and optimized processing conditions by resizing the images. A lightweight parallel depth-wise separable CNN (LPDCNN) was developed to extract essential image features. This advanced neural network architecture can encode 200 discriminant features, resulting in accurate malaria classification. Using this foundation, Traditional Extreme Learning Machine (TELM) and RELM

model was created, which performs better in distinguishing infected cells from uninfected cells. An explanatory strategy based on the SHAP method revealed the LPDCNN-RELM model's inner workings. This innovative visualization technique highlights the most influential characteristics contributing to the classification outcomes, providing valuable insights into the model's decision-making process. Overall, this hybrid framework combines cutting-edge techniques to achieve effective malaria detection and help us understand the classification process better.

The following sections comprehensively explain the methodology utilized in crafting the proposed framework. The framework has undergone substantial improvements, resulting in a noteworthy boost in the precision and accuracy of malaria detection in RBC cell images.

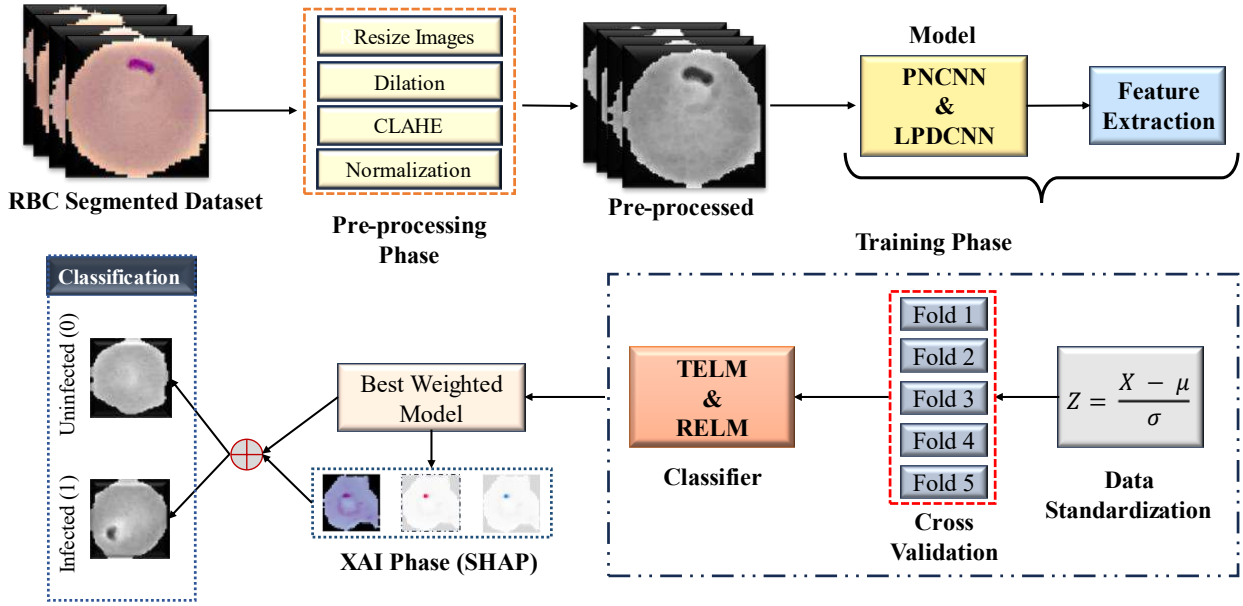

Figure 1. Proposed framework for malaria classification from RBC segmented images.

2.2 Dataset Collection

The dataset utilized in the study was obtained from RBC-segmented images, which can be accessed via the National Library of Medicine: https://lhncbc.nlm.nih.gov/LHC-downloads/downloads.html#malaria-datasets. Rajaraman et al. [17] created the dataset in their research, where they developed a segmentation process to differentiate RBC images from thin blood smear images. The dataset comprises 27,588 images, categorized into two groups: infected and uninfected. This dataset is balanced which comprises 13,779 images in the infected category displaying the malaria parasite and 13,779 images in the uninfected category without the parasite. However, there was some mislabeling in this data, such as infected cells being placed in the uninfected class. In their study, Fuhad et al. [26] relied on medical professionals to provide a manual solution. Based on their research, they determined that 647 and 750 false positives were infected and uninfected. The total samples were 26,161, containing 13,029 uninfected and 13,132 infected images. A rigorous evaluation strategy was implemented on this modified dataset to ensure the model's reliability and validity, incorporating the highly regarded five-fold cross-validation (CV) method, known for its robustness and significance in determining the model's effectiveness. The research findings are trustworthy and credible due to the use of this method. A few examples of images from the dataset are displayed in Figure 2.

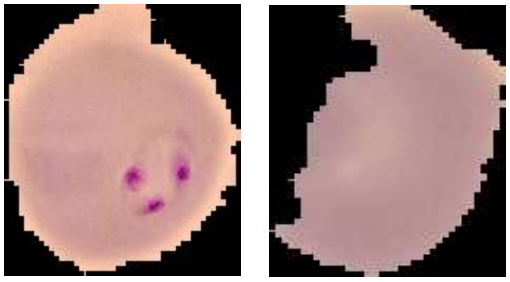

(A) (B)

Figure 2. Samples of blood smear which contain (A) infected cell, and (B) uninfected cell.

2.3 Image Preprocessing

Optimizing a classification model's performance heavily relies on image preprocessing quality. In order to achieve this, we begin by reducing the width and vertical dimensions of the image to 32×32 pixels. We combine well-known techniques such as Dilation (a morphological operation) and CLAHE to enhance the image preprocessing strategy further. Dilation is a highly effective method that connects fragmented images, resulting in a continuous and coherent representation of image components. This technique not only enhances the shapes of entities but also highlights specific structures or features, ultimately improving the overall interpretability of the processed image. In addition, Dilation has the added benefit of effectively reducing noise and unwanted artifacts, making it a crucial component in our hybrid preprocessing strategy.

Preprocessing techniques have the power to eliminate unwanted noise from an image while still maintaining crucial object details. This results in a sharper and more refined image, ideal for further analysis. In both skeletonization and thinning processes, dilation is vital, reducing object thickness to its central axis while preserving connectivity [33]. Skeletonized representations be helpful for tasks relating to shape analysis and pattern recognition. By enhancing the representation of specific patterns or structures within an image, dilation significantly boosts the efficacy of pattern-matching algorithms and feature extraction techniques. In our research, we have utilized dilatation to reduce noise in human blood cells, resulting in more explicit images and improved visibility of anatomical details like microscopic cells and airways. Hematologists can significantly improve the accuracy of blood cell diagnoses with this technology. Furthermore, we have employed the advanced image enhancement technique, CLAHE, to dynamically redistribute intensity values, improving contrast and refining image quality [34]**.** The CLAHE technique is a highly effective method for improving the detection of infections. This technique reduces noise and improves tissue distinction in the blood by applying histogram equalization to smaller sections of an image rather than globally over the entire image. With this, even minor infections can be identified more accurately. Furthermore, normalizing the images by dividing them by 255 simplifies subsequent analysis and significantly reduces the computational complexity of the model. Hematologists can confidently rely on this technique to improve the accuracy of malaria detection. Using dilatation and CLAHE procedures enhances the readability of human blood cells, thus allowing for a more precise diagnosis of malaria detection. With the CLAHE technique, local contrast is boosted, and tiny anomalies are highlighted, while dilation efficiently eliminates noise without compromising crucial image properties. Figure 3, demonstrates the before and after preprocessed samples.

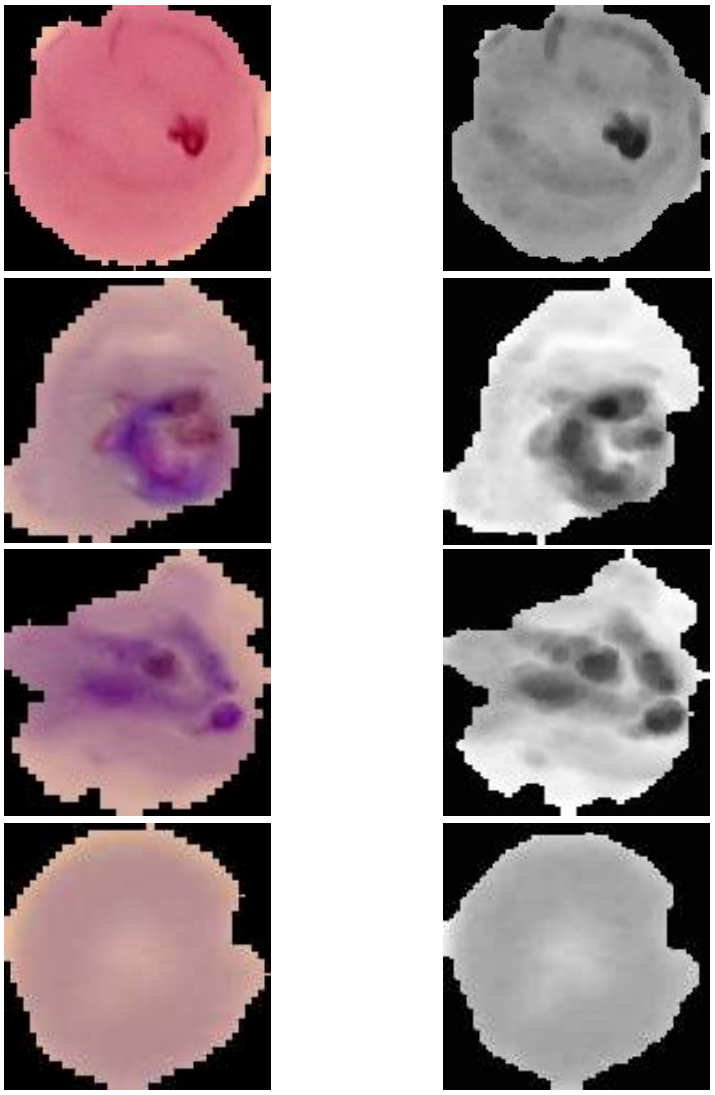

(A) (B)

Figure 3. RBC segmented images (A) before and (B) after Dilation and CLAHE preprocessing.

2.4 Lightweight Parallel Depthwise Separable Convolutional Neural Network (LPDCNN)

Our main goal was to create a lightweight CNN model that could effectively detect important features while also being compact and practical in size. To achieve this, we developed a simplified LPDCNN model that balances layer complexity and parameter constraints**. Figure 4** displays the architecture of this lightweight model, which elegantly extracts distinct features from RBC-segmented images. To make the CNN model more accessible than Transfer Learning (TL), we utilized a more nuanced approach. The model comprises 8 convolution layer (CL) and 2 fully connected layers (FC), carefully crafted to attain the perfect balance. Using only one CL would overlook crucial details, while incorporating five consecutive CLs would add unnecessary depth and complexity [24].

We executed the initial five convolutional layers (CLs) simultaneously through concatenation and extensive experimentation. With 256 kernels in each CL, ranging from 11×11 to 3×3, we ensured maximum feature extraction and precise classification. By applying consistent padding to the first five CLs, we obtained complete data extraction from all regions, including border areas. The parallel CLs produced feature maps that were later combined and processed further through a sequential CL**.**

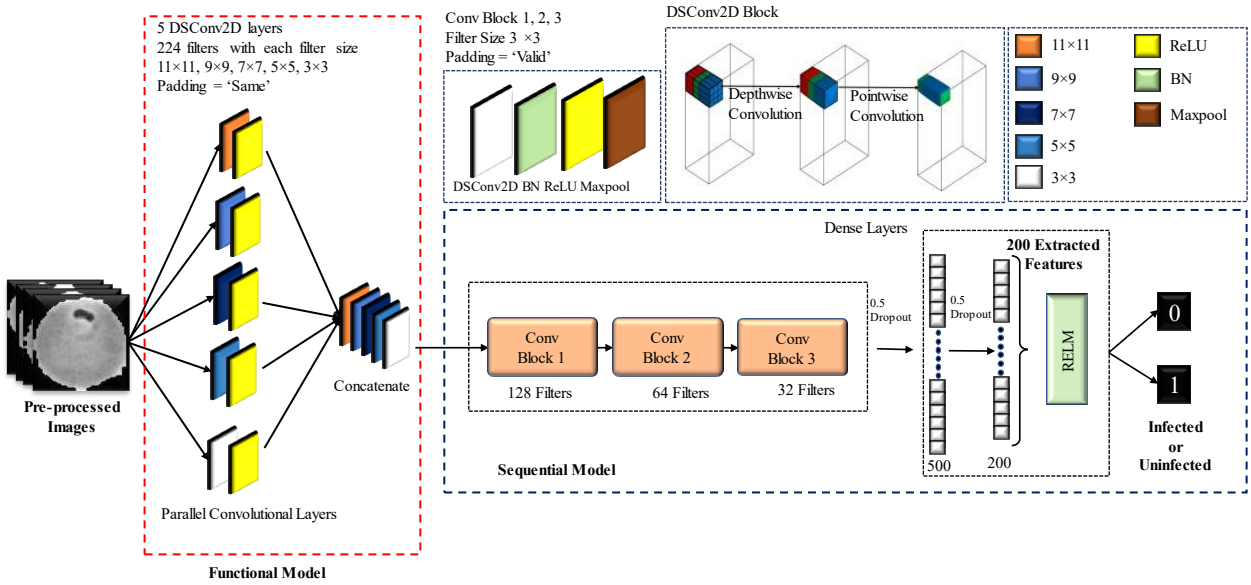

Figure 2. Proposed LPDCNN architecture for feature extraction (*DSConv2D: depthwise separable convolution and BN: batch normalization).

We employed the depthwise separable convolution (DSC) technique to streamline the model while maintaining its classification efficiency. DSC divides the convolution process into two parts - depthwise and pointwise convolution - which significantly reduced the number of parameters needed from 19.54 million to 0.36 million. In order to enhance accuracy, we added a batch normalization (BN) layer and a max-pooling layer after the preceding three CLs, each with 3×3 kernels and the appropriate padding. We selected optimal sizes of filters 128, 64, and 32 for these layers. In detail, model summary with parameters of each layer are presented at Table 2.

BN has improved the model to make it faster and more reliable. To ensure consistency and non-linearity during training, all CLs utilized the rectified linear unit (ReLU) activation function [35]. In order to prevent overfitting and speed up training, we utilized dropout layers with a 0.5 probability of ignoring half of the nodes in the network. Specifically, a dropout layer was added after the first FC layer and another after the last two CLs. We utilized the ADAM optimizer's 0.001% learning rate with 100 epochs and the sparse categorical cross-entropy loss function to extract features as the model loss. We selected 200 unique features from the last FC layer through trial and error to determine the model's capabilities.

The features were first standardized using the standard scaler to improve the accuracy of the ELM model's analysis. This transformation adjusted the feature values to a standardized scale, enabling

the ELM model to process the data effectively. The standardized features allowed the ELM model to perform more accurately and efficiently [36].

$$y = \frac{x - \bar{x}}{\sigma} \quad (1)$$

Where, $\bar{x}$ = Mean of the samples,

σ = Standard deviation of the samples.

Table 2. Lightweight parallel depthwise separable convolutional neural network (LPDCNN) model summary.

Layer Type	Output Shape	Params
model_1 (Functional)	(None, 32, 32, 1280)	5975
separable_conv2d_	(None, 30, 30, 128)	175488
batch_normalization	(None, 30, 30, 128)	512
activation_	(None, 30, 30, 128)	0
max_pooling2d	(None, 15, 15, 128)	0
separable_conv2d	(None, 13, 13, 64)	9408
batch_normalization	(None, 13, 13, 64)	256
activation	(None, 13, 13, 64)	0
max_pooling2d_	(None, 6, 6, 64)	0
separable_conv2d	(None, 4, 4, 32)	2656
batch_normalization	(None, 4, 4, 32)	128
activation	(None, 4, 4, 32)	0
max_pooling2d	(None, 2, 2, 32)	0
flatten (Flatten)	(None, 128)	0
dense (Dense)	(None, 500)	64500
batch_normalization	(None, 500)	2000
dropout (Dropout)	(None, 500)	0
DenseLastML (Dense)	(None, 200)	100200

2.5 Ridge Regression Extreme Learning Machine (RELM)

The ELM, introduced by Huang et al. [37], is an exceptional paradigm that has revolutionized feature classification. It uses a forward feed network based on the principles of supervised learning, making it a novel contribution. By utilizing the power of neural networks (NN), ELM has eliminated the need for backpropagation, resulting in a remarkable thousand-fold acceleration in training times. This revolutionary development has given the model unparalleled generalization capabilities and classification performance. Notably, ELM has proven remarkably proficient in large-scale binary classification, surpassing conventional techniques [38]. ELM ingeniously and arbitrarily initializes the parameters connecting the input and hidden layers by employing a single hidden layer. The parameters connecting the concealed and output layers were determined using the pseudoinverse technique. In this study, however, a new level of sophistication was introduced by substituting the pseudoinverse method with the hybrid ridge regression technique. This enhancement improved the model's capacity for effective feature learning and regularization,

thereby enhancing its capacity for generalization and delivering unprecedented accuracy compared to the traditional ELM. The model architecture featured a remarkable collection of 200 nodes in the input layer, while the hidden layer featured a formidable collection of 100 nodes. Two nodes comprised with the RELM algorithm then output layer, crucial for classifying distinct types of infected and uninfected patients' samples from RBC smear images. The explanation of the hybrid RELM algorithm is given below:

Algorithm 1: Hybrid Ridge Regression ELM (RELM) algorithm for malaria infected RBC image classification

$$X_{(n,m)} = \begin{bmatrix} x_{(1,1)} & x_{(1,2)} & \cdots & x_{(1,m)} \\ x_{(2,1)} & x_{(2,2)} & \cdots & x_{(2,m)} \\ x_{(3,1)} & x_{(3,2)} & \cdots & x_{(2,m)} \\ \vdots & \vdots & \ddots & \vdots \\ x_{(n,1)} & x_{(n,2)} & \cdots & x_{(n,m)} \end{bmatrix} \quad Y_{(n,t)} = \begin{bmatrix} y_{(1,1)} & y_{(1,2)} & \cdots & y_{(1,t)} \\ y_{(2,1)} & y_{(2,2)} & \cdots & y_{(2,t)} \\ y_{(3,1)} & y_{(3,2)} & \cdots & y_{(3,t)} \\ \vdots & \vdots & \ddots & \vdots \\ y_{(n,1)} & y_{(n,2)} & \cdots & y_{(n,t)} \end{bmatrix}$$

Let X and Y denote the input and output matrices, respectively.

1. The input weight $W_{(m,N)}$ and bias $B_{(1,N)}$ matrices are first generated at random.

$$W_{(m,N)} = \begin{bmatrix} w_{(1,1)} & w_{(1,2)} & \cdots & w_{(1,N)} \\ w_{(2,1)} & w_{(2,2)} & \cdots & w_{(2,N)} \\ w_{(3,1)} & w_{(3,2)} & \cdots & w_{(3,N)} \\ \vdots & \vdots & \ddots & \vdots \\ w_{(m,1)} & w_{(m,2)} & \cdots & w_{(m,N)} \end{bmatrix}$$

$$B_{(1,N)} = \begin{bmatrix} b_{(1,1)} & b_{(1,2)} & \cdots & b_{(1,N)} \end{bmatrix}$$

2. The second step is to find the output $H_{(n,N)}$ of the hidden layer.

$$H_{(n,N)} = G(X_{(n,m)} \cdot W_{(m,N)} + B_{(1,N)})$$

$$H(n,N) = \begin{bmatrix} h_{(1,1)} & h_{(1,2)} & \cdots & h_{(1,N)} \\ h_{(2,1)} & h_{(2,2)} & \cdots & h_{(1,N)} \\ h_{(3,1)} & h_{(3,2)} & \cdots & h_{(1,N)} \\ \vdots & \vdots & \ddots & \vdots \\ h_{(n,1)} & h_{(n,2)} & \cdots & h_{(n,N)} \end{bmatrix}$$

Where, G denotes an activation function in this context.

3. Determine the output weight matrix $\beta_{(N,t)}$ using pseudoinverse

$$\beta_{(N,t)} = H^{\dagger}_{(N,n)} \cdot T_{(n,t)}$$

In this proposed hybrid Ridge regression, the pseudoinverse has been replaced by these equations:

$$\boldsymbol{A_{(N,N)} = H^{T}_{(N,n)} \cdot H_{(n,N)}}$$

$$\boldsymbol{b_{(N,t)} = H^{T}_{(N,n)} \cdot T_{(n,t)}}$$

$$\boldsymbol{C_{(N,N)} = A_{(N,N)} + \alpha . I_{(N,N)}}$$

$$\boldsymbol{B_{(N,t)} = C^{-1}_{(N,N)} \cdot b_{(N,t)}}$$

Where, α denotes regularization parameters.

4. Make prediction using $\beta_{(N,t)}$.

The model radiated assurance that it would produce the final predictions with exceptional precision. RELM, a methodology that seamlessly integrated Ridge Regression within the ELM framework, established an exquisite balance between potent feature learning and regularization. The model's ability to generalize and decipher complex patterns in the data improved as a result, taking its prediction power to new heights. Figure 5, presents the RELM model architecture in binary classification.

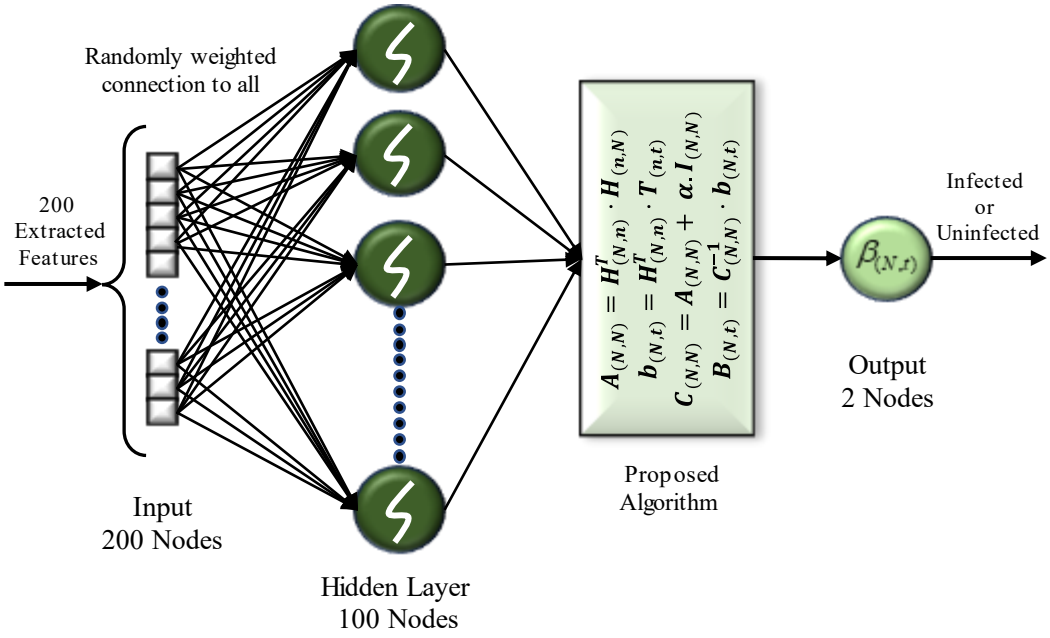

Figure 5. Proposed RELM architecture.

2.6 Classification Matrices and Loss Function

To assess the classification performance of the RELM model, we utilized confusion matrices (CMs). These matrices are known for their effectiveness in evaluation. By applying the equations, we calculated various metrics such as accuracy, precision, recall, f1-score, and area under the curve (AUC) [39].

$$Accuracy = \frac{T_P + T_N}{T_P + T_N + F_P + F_N} \tag{2}$$

$$Precision = \frac{T_P}{T_P + F_P} \tag{3}$$

$$Recall = \frac{T_P}{T_N + F_P} \tag{4}$$

$$F1 - Score = \frac{2 \times (Precision \times Recall)}{Precision + Recall} \tag{5}$$

$$AUC = \frac{1}{2}\left(\frac{T_P}{T_P + F_N} + \frac{T_N}{T_N + F_P}\right) \tag{6}$$

Where, T_P = True positive, T_N = True negative, F_P = False positive, and F_N = False negative.

The cross-entropy formula compares the actual class label (expressed as integers) to the model's projected probability distribution. The cross-entropy loss, a metric for assessing how different the actual labels are from the expected ones, must be kept as little as possible. Numerous deep-learning applications, including image classification and natural language processing, use the sparse categorical cross-entropy loss because it performs well in situations with multiple classes [40]. Here's the formula:

$$L_{ce} = -\sum_{i=1}^{n} t_i \times \log(p_i) \tag{7}$$

Where, n is the class number, truth label is defined as t_i, and p_i as the probability.

3. Experiment Analysis

This research utilizes a hybrid method that significantly enhances malaria categorization. Two powerful algorithms were compared to achieve accurate malaria classification: Traditional Extreme Learning Machines (TELM) and Ridge Regression Extreme Learning Machines (RELM). The study begins by improving image quality by combining CLAHE and dilatation techniques. The most significant features of the images are extracted simultaneously using parallel normal CNN (PNCNN) and lightweight parallel depth-wise CNN (LPDCNN) models. These extracted features are standardized and then inputted into ELM models for analysis.

A PNCNN is a neural network that uses multiple connectivity levels, including convolutional, pooling, and FC layers. Each convolutional layer works simultaneously to extract features from the input data at various levels of abstraction. These combined features are then used in deeper neural network layers. An LPDCNN is another type of neural network that maximizes efficiency by using parallel processing to minimize computational complexity. It uses Depthwise Separable Convolutions, which break up the conventional convolution into depthwise convolution (filtering each input channel independently) and pointwise convolution (aggregating the output channels using a 1×1 convolution). By reducing unnecessary parameters and computations, this type of network is more compact and faster than others.

3.1 Results of TELM and proposed RELM with PNCNN model

Figures 6A and 6B display the accuracy and loss curves of PNCNN. During training and validation, the categorization performance achieved an accuracy of 99.97% and 98.48%. At the final epochs, the training and validation losses were 0.102% and 0.152%, respectively.

Table 3 showcases the remarkable differences in performance between TELM and RELM in the PNCNN framework. The accuracy of the models was tested through a rigorous five-fold cross-validation technique on various subsets of data, ensuring their reliability**.** Figures 7 and 8 provide critical insights into the classification results through the CMs for TELM and RELM, respectively. The matrices calculate essential metrics such as class-wise precision, recall, and f1-score. RELM secured an impressive average precision of 99.26%±0.336 at ELM in several categories, while TELM achieved 99.34%±0.321 with an improvement of 0.081%. Furthermore, RELM exhibited a boost of about 0.061% in average recall and f1-score, leading to an overall increase of 0.081% in the accuracy of the PNCNN model.

The ROC AUC performance of TELM and RELM are demonstrated in Figure 9 and 10, respectively. The data reveals that RELM efficiently separates malaria from segmented RBC samples. RELM has the highest AUC value of 99.81%, surpassing TELM's AUC of 99.80%. These results provide robust evidence for the practicality of the suggested RELM technique. It demonstrates significant performance in helping medical professionals diagnose malaria cases accurately based on RBC images. In conclusion, this analysis proposes a novel hybrid RELM model that outperforms the conventional ELM method on the PNCNN model regarding performance and accuracy.

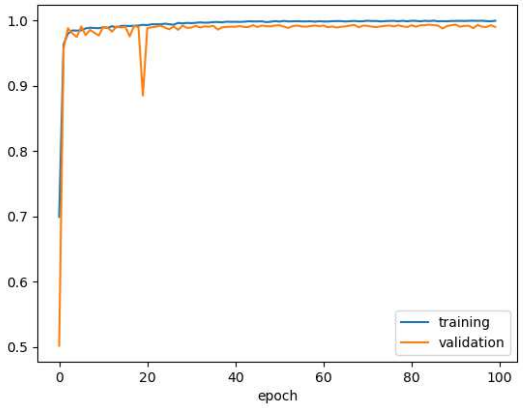

(A)

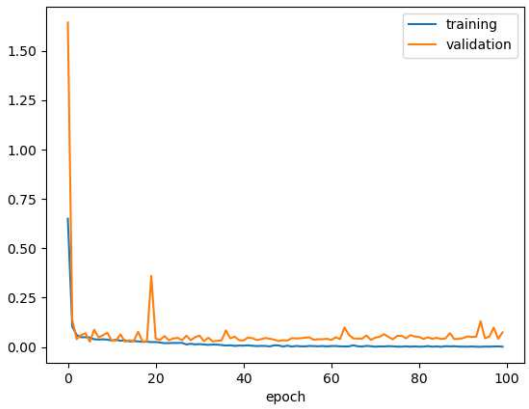

(B)

Figure 6. PNCNN model curves which include (A)Training validation accuracy, and (B) loss curve.

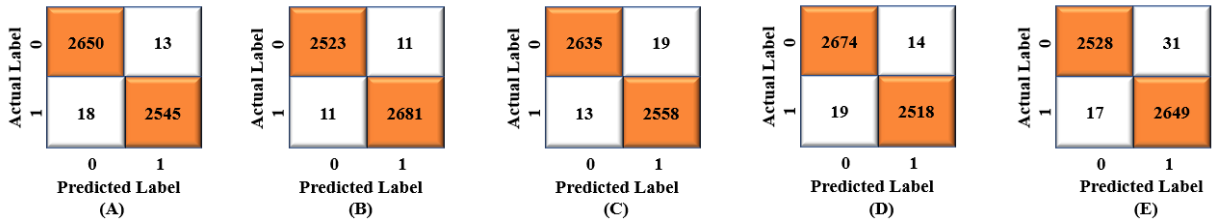

Figure 7. CMs of PNCNN-TELM models on (A) fold 1, (B) fold 2, (C) fold 3, (D) fold 4, and (E) fold 5 for malaria classifications.

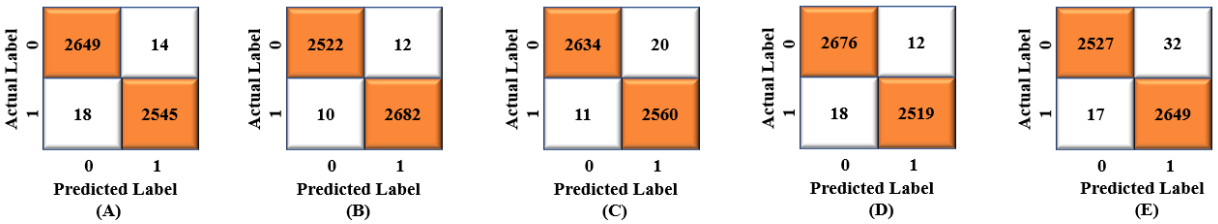

Figure 8. CMs of PNCNN-RELM model on (A) fold 1, (B) fold 2, (C) fold 3, (D) fold 4, and (E) fold 5 for malaria classifications.

Table 3. Class-wise classification performances on PNCNN with TELM and RELM for five folds CV.

Fold Numbe	Classes	Precision		Recall		F1-score		Accuracy (%)		AUC (%)	
		TELM	RELM	TELM	RELM	TELM	RELM	TELM	RELM	TELM	RELM
Fold 1	Infected (0)	0.99	0.99	1.00	0.99	0.99	0.99	-	-	**99.73**	99.72
	Uninfected (1)	0.99	0.99	0.99	0.99	0.99	0.99	-	-		
	Average	0.995	**0.995**	0.993	**0.993**	0.994	**0.994**	99.40	**99.39**		
Fold 2	Infected (0)	1.00	1.00	1.00	1.00	1.00	1.00	-	-	**99.84**	99.83
	Uninfected (1)	1.00	1.00	1.00	1.00	1.00	1.00	-	-		
	Average	0.995	0.995	0.995	**0.996**	0.995	**0.996**	99.57	**99.58**		
Fold 3	Infected (0)	1.00	1.00	0.99	0.99	0.99	0.99	-	-	**99.84**	99.80
	Uninfected (1)	0.99	0.99	0.99	1.00	0.99	0.99	-	-		
	Average	0.992	**0.993**	0.995	**0.996**	0.994	**0.994**	99.38	**99.41**		
Fold 4	Infected (0)	0.99	0.99	0.99	1.00	0.99	0.99	-	-	99.92	**99.94**
	Uninfected (1)	0.99	1.00	0.99	0.99	0.99	0.99	-	-		

	Average	0.994	**0.996**	0.992	**0.993**	0.993	**0.994**	99.36	**99.43**		
Fold 5	**Infected (0)**	0.99	0.99	0.99	0.99	0.99	0.99	-	-	99.69	**99.74**
	Uninfected (1)	0.99	0.99	0.99	0.99	0.99	0.99	-	-		
	Average	0.987	**0.988**	0.993	**0.993**	0.990	**0.991**	**99.08**	99.06		
Average (μ)±SD (σ) (%)		99.26 ±0.33 6	**99.34± 0.321**	99.36 ±0.13 4	**99.42±0 .164**	99.32 ±0.19 2	**99.38± 0.178**	99.30± 0.187	**99.38±0 .178**	99.80 ±9.20 3	**99.81 ±8.70 6**

*Bold values indicate best results.

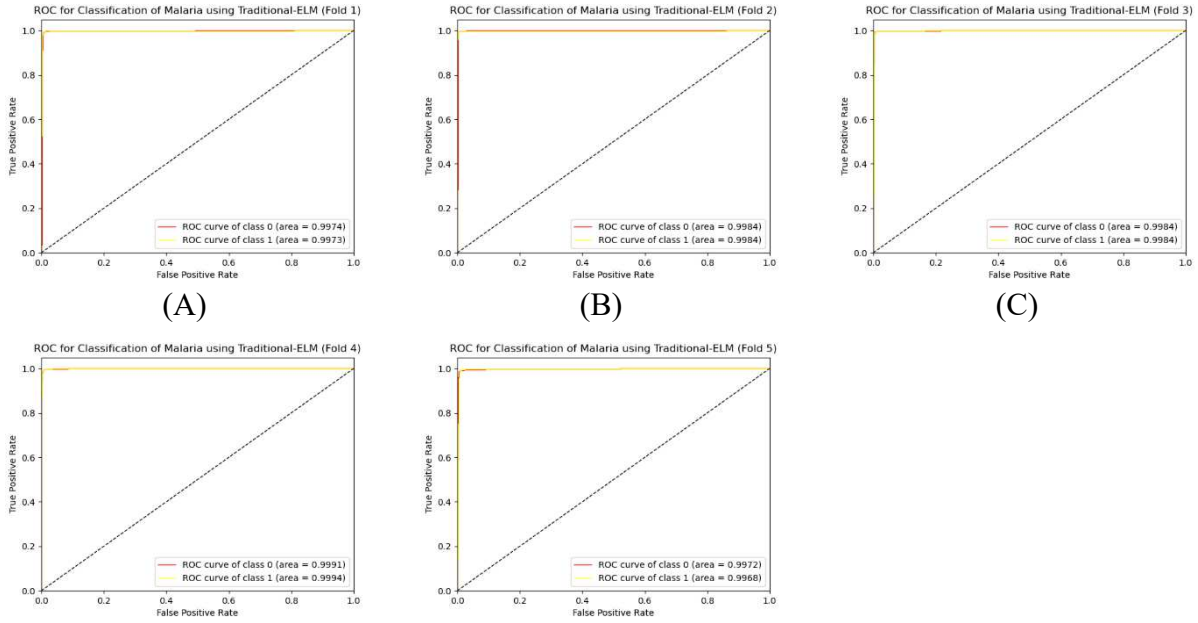

Figure 9. Class-wise ROCs of PNCNN-TELM on (A) fold 1, (B) fold 2, (C) fold 3, (D) fold 4, and (E) fold 5 for multiclass classification.

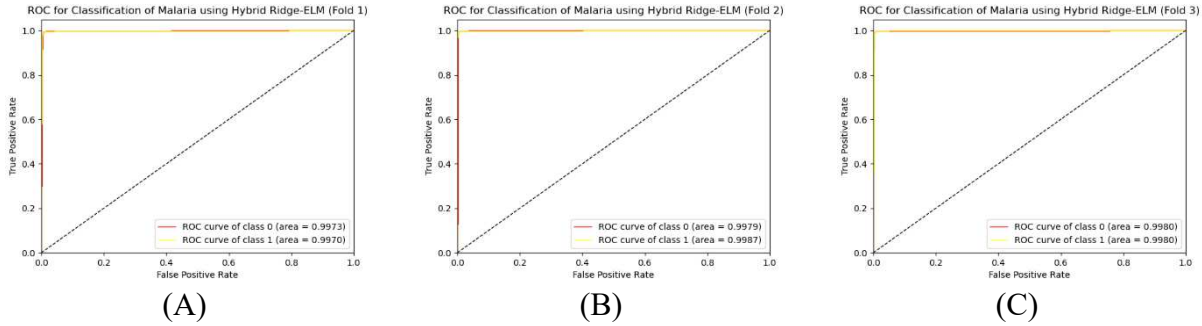

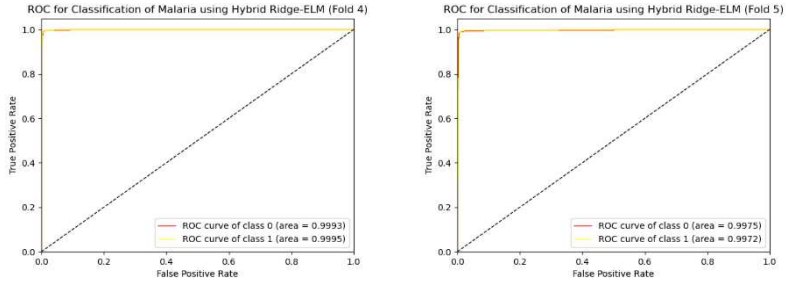

(D) (E)

Figure 10. Class-wise ROCs of PNCNN-RELM on (A) fold 1, (B) fold 2, (C) fold 3, (D) fold 4, and (E) fold 5 for multiclass classification.

3.2 Results of TELM and proposed Hybrid RELM (RELM) with LPDCNN model

Figures 11A and 11B display the model accuracy and loss curve scores. The training accuracy score was 99.98%, while the validation accuracy score was 98.82%. The loss curve scores were 0.096% and 0.121% for training and validation, respectively.

For the malaria dataset, we effectively applied the LPDCNN architecture alongside TELM and RELM. The classification outputs were ensured by testing the models on multiple dataset subsets using a strict five-fold CV method. We highlighted the generated confusion matrices in Figure 12 and 13, alongside the crucial evaluation metrics, including class-wise precision, recall, f1-score, and AUC which are meticulously calculated and presented in Table 4.

However, we have successfully developed a hybrid RELM model to enhance performance across all folds. The results are optimistic, with the hybrid RELM model surpassing TELM by a significant margin in Fold 2. The RELM achieved an extraordinary f1-score of 99.90% (a gain of 0.10%) and a precision of approximately 99.90% (an overall improvement of 0.10% over TELM). Furthermore, RELM demonstrates remarkable performance in terms of precision, recall, f1, and accuracy, with scores of 99.86%±0.08, 99.88%±0.084, 99.84%±0.089, and 99.85%±0.071, respectively.

The hybrid RELM model has far surpassed expectations, boasting a stunning precision, recall, and accuracy rate of 99% each fold. This remarkable performance is an incredible 0.08% improvement (99.86%±0.081) from TELM, providing indisputable evidence of the superiority of the hybrid RELM technique. Figures 14 and 15 provide conclusive class-wise ROC curves. These illustrations unequivocally prove that RELM outperforms TELM in differentiating between RBC-segmented cells and those infected with malaria, with an astounding AUC value of 99.96% compared to TELM's 99.95%. These results establish the hybrid RELM model as a potential game-changer in medical haematology, as it can aid in accurately identifying malaria infection using segmented images. In conclusion, this study has introduced the innovative RELM model as an improved approach then TELM, offering superior accuracy and precision in each fold and emerging as the new gold standard for malaria classification.

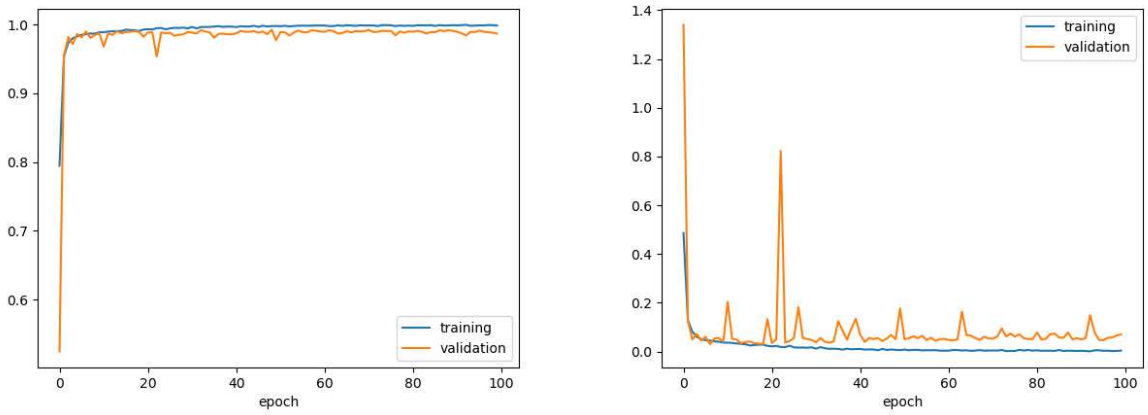

Figure 11. LPDCNN model curves which include (A)Training validation accuracy, and (B) loss curve.

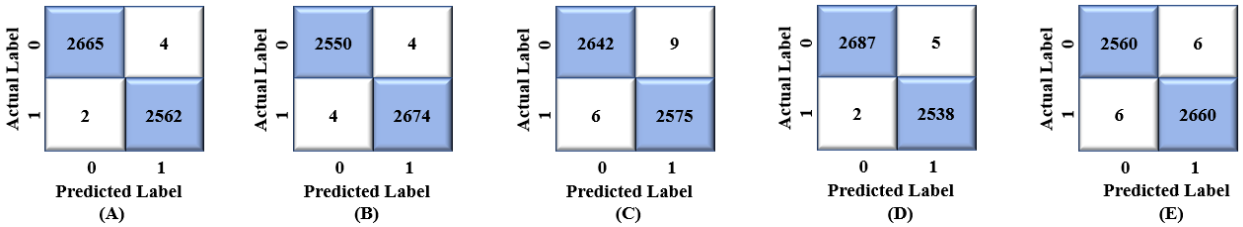

Figure 12. CMs of LPDCNN-TELM on (A) fold 1, (B) fold 2, (C) fold 3, (D) fold 4, and (E) fold 5 for multiclass classifications.

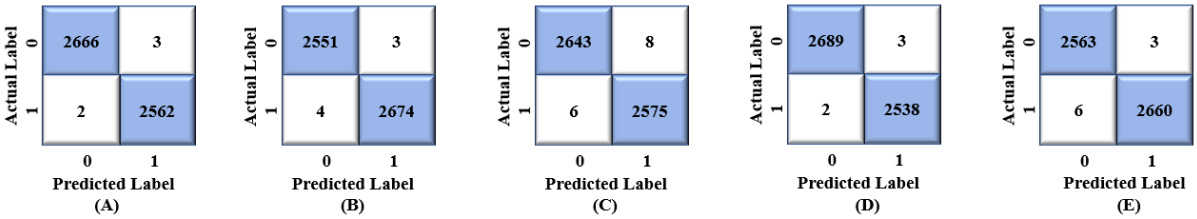

Figure 13. CMs of LPDCNN-RELM on (A) fold 1, (B) fold 2, (C) fold 3, (D) fold 4, and (E) fold 5 for multiclass classifications.

Table 4. Class-wise classification performances on LPDCNN with TELM and RELM for five folds CV.

Fold Number	Diseases Class	Precision		Recall		F1-score		Accuracy (%)		AUC (%)	
		TELM	RELM	TELM	RELM	TELM	RELM	TELM	RELM	TELM	RELM
Fold 1	Infected (0)	1.00	1.00	1.00	1.00	1.00	1.00	-	-	99.99	**99.99**
	Uninfected (1)	1.00	1.00	1.00	1.00	1.00	1.00	-	-		

	Average	0.998	**0.999**	0.999	**0.999**	0.998	**0.999**	99.88	**99.90**		
Fold 2	**Infected (0)**	1.00	1.00	1.00	1.00	1.00	1.00	-	-	99.92	**99.99**
	Uninfected (1)	1.00	1.00	1.00	1.00	1.00	1.00	-	-		
	Average	0.998	**0.999**	0.998	**0.998**	0.998	**0.999**	99.84	**99.87**		
Fold 3	**Infected (0)**	1.00	1.00	1.00	1.00	1.00	1.00	-	-	**99.92**	99.90
	Uninfected (1)	1.00	1.00	1.00	1.00	1.00	1.00	-	-		
	Average	0.996	**0.997**	0.997	**1.00**	0.997	**0.997**	99.71	**99.73**		
Fold 4	**Infected (0)**	1.00	1.00	1.00	1.00	1.00	1.00	-	-	**99.99**	99.96
	Uninfected (1)	1.00	1.00	1.00	1.00	1.00	1.00	-	-		
	Average	0.998	**0.999**	0.999	**0.999**	0.998	**0.999**	99.86	**99.90**		
Fold 5	**Infected (0)**	1.00	1.00	1.00	1.00	1.00	1.00	-	-	99.96	**99.97**
	Uninfected (1)	1.00	1.00	1.00	1.00	1.00	1.00	-	-		
	Average	0.997	**0.999**	0.997	**0.998**	0.997	**0.998**	99.77	**99.83**		
Average (μ)±SD (σ) (%)		99.74± 0.08	**99.86± 0.08**	99.80± 0.10	**99.88± 0.084**	99.76±0 .055	**99.84±0 .089**	99.81± 0.070	**99.85± 0.071**	99.95 ±0.03 5	**99.96±0 .037**

*Bold values indicate best results.

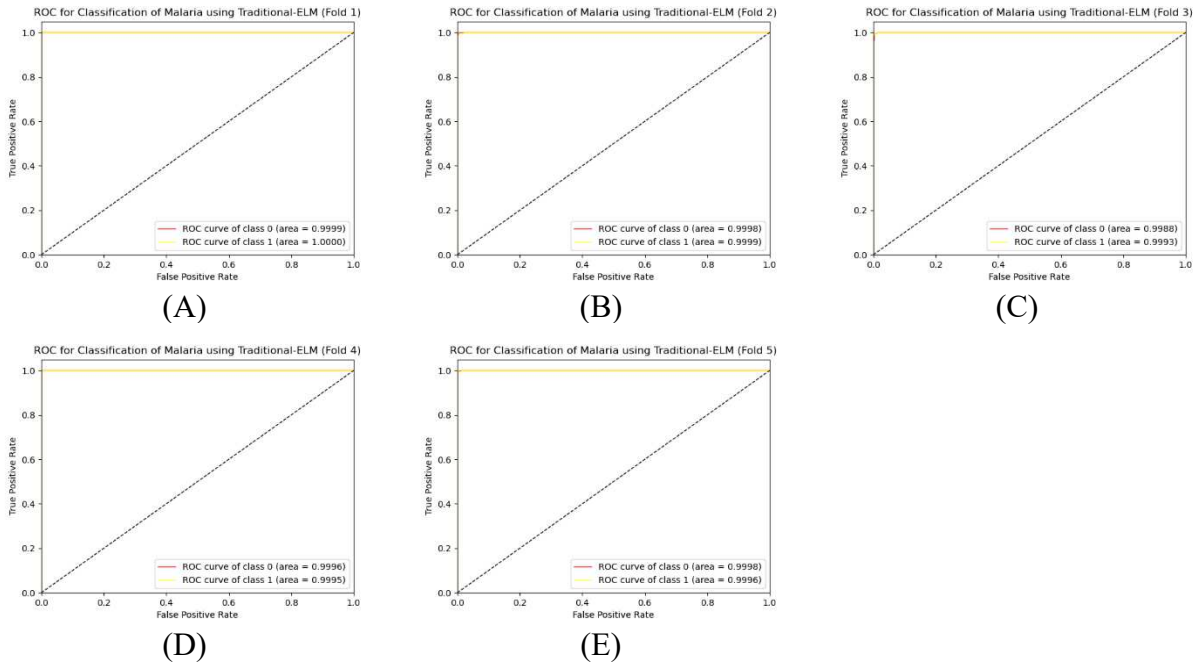

Figure 14. Class-wise ROCs of LPDCNN-TELM on (A) fold 1, (B) fold 2, (C) fold 3, (D) fold 4, and (E) fold 5.

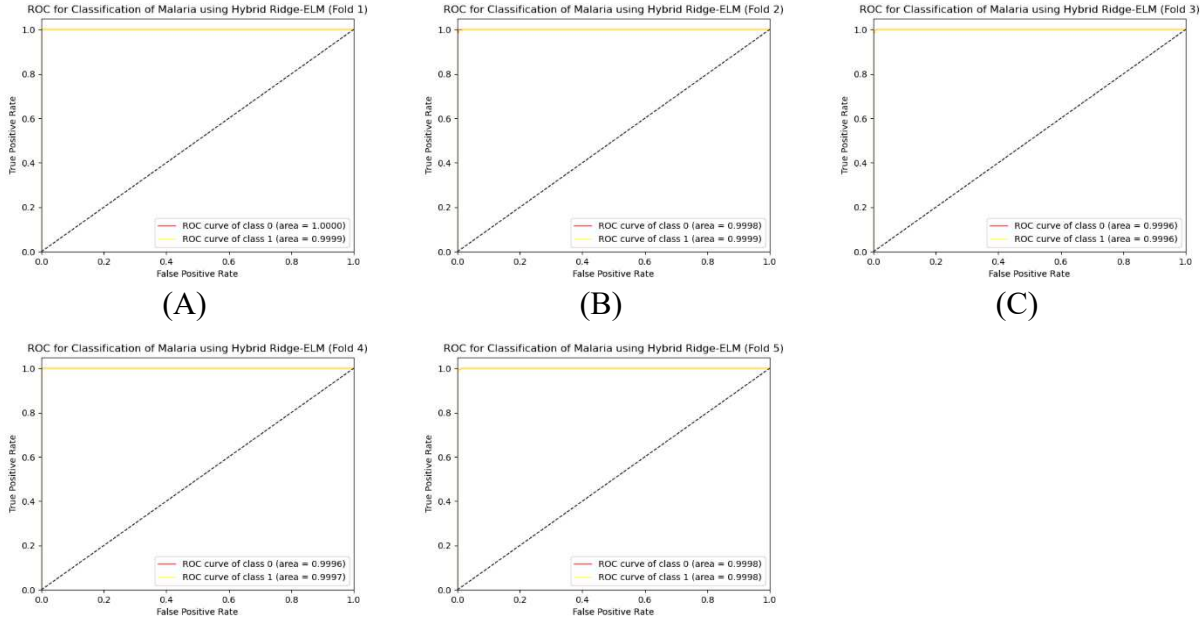

Figure 15. Class-wise ROCs of LPDCNN-RELM on (A) fold 1, (B) fold 2, (C) fold 3, (D) fold 4, and (E) fold 5.

3.3 Performances comparisons among proposed model with other SOTA ML Models

A comprehensive study was conducted to compare the performance of the latest State-of-the-Art (SOTA) ML models, with the hybrid RELM model being identified as a remarkable feature extractor. The study incorporated six well-known ML models, including Support Vector Machine (SVM), Gaussian Naive Bayes (GNB), Decision Tree (DT), and XG-Boost, all of which were integrated into the LPDCNN framework (as its best model found in result analysis). The study extracted the top 200 features using each ML model, which were then fed into the innovative RELM for further analysis. The LPDCNN-RELM method was evaluated using various metrics, including classification mean precision, recall, f1-score, accuracy, and AUC, in comparison to other models. The ML models were trained using the robust five-fold CV technique to ensure accurate and objective results. The best results for each model are highlighted to provide a clear presentation without compromising analytical rigor.

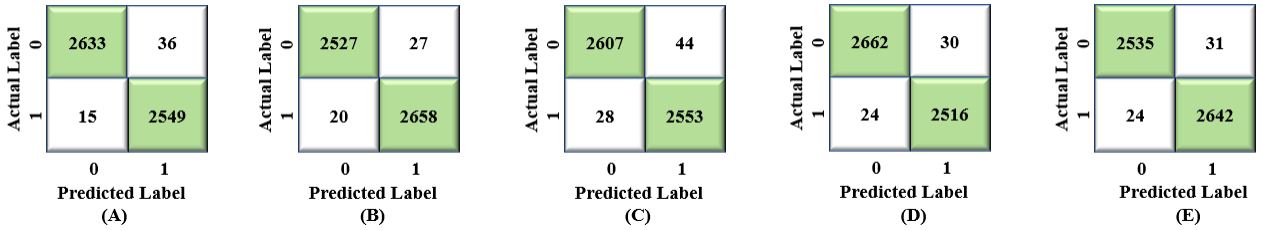

Figure 16. CMs of LPDCNN-SVM on (A) fold 1, (B) fold 2, (C) fold 3, (D) fold 4, and (E) fold 5 for malaria classifications.

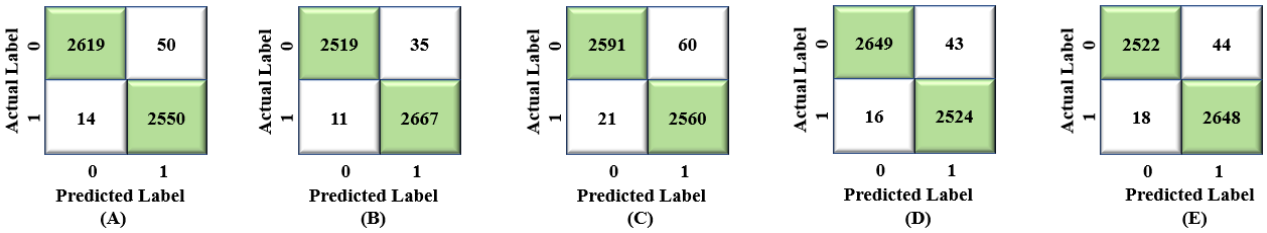

Figure 17. CMs of LPDCNN-GNB on (A) fold 1, (B) fold 2, (C) fold 3, (D) fold 4, and (E) fold 5 for malaria classifications.

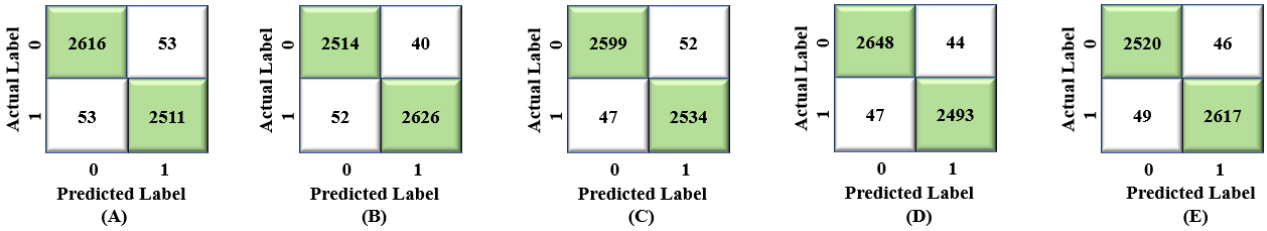

Figure 18. CMs of LPDCNN-DT on (A) fold 1, (B) fold 2, (C) fold 3, (D) fold 4, and (E) fold 5 for malaria classifications.

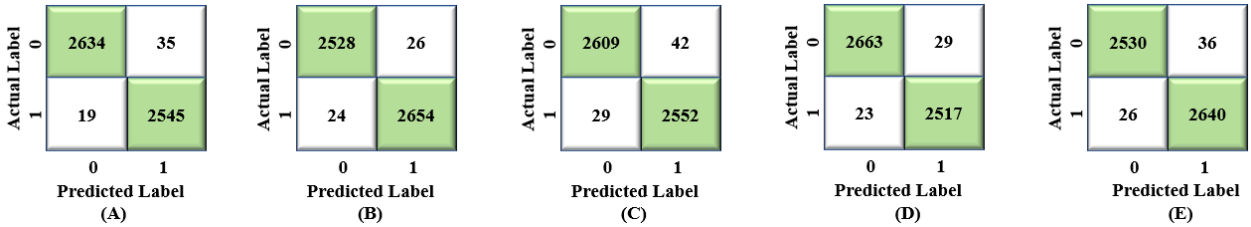

Figure 19. CMs of LPDCNN-XG-Boost on (A) fold 1, (B) fold 2, (C) fold 3, (D) fold 4, and (E) fold 5 for malaria classifications.

The CMs of six ML models tested on the same CV dataset are presented in Figures 16, 17, 18 and 19. As per Table 5, the LPDCNN-RELM model outperforms the others concerning average precision, recall, and f1-score, exceeding 99.9%. Notably, the AUC for PNCNN+RELM was 99.94%, while LPDCNN-RELM scored the highest at 99.99%. Corresponding ROC curves for each model on the CV test set are displayed in Figures 20, 21, 22 and 23. Although LPDCNN-SVM exhibited superior classification levels in precision and recall compared to other ML techniques, it still needs to enhance its discriminative abilities, which LPDCNN-RELM. This difference is further highlighted by the AUC curves, which reveal that LPDCNN achieved an approximate ROC of 99.99%, whereas DT only achieved lowest AUC score 98.20%. These findings demonstrated that our suggested LPDCNN is highly reliable for malaria classification and that combining it with the hybrid RELM technique further boosts the detection rate.

Table 5. Comparative classification performances on SOTA models.

CV		PNCNN-ELM	PNCNN-RELM	LPDCNN-ELM	LPDCNN-RELM	LPDCNN -SVM	LPDCNN -GNB	LPDCNN -DT	LPDCNN -XGBoost
Fo	mP	0.995	0.995	0.998	**0.999**	0.986	0.981	0.980	0.986
	mR	0.993	0.993	0.999	**0.999**	0.994	0.994	0.980	0.992

	mF1	0.994	0.994	0.998	**0.999**	0.990	0.987	0.980	0.989
	mACC (%)	99.40	99.39	99.88	**99.90**	99.02	98.77	97.97	98.96
	AUC (%)	99.73	99.72	99.99	**99.99**	99.45	98.90	97.97	99.84
Fold 2	mP	0.995	0.995	0.998	**0.999**	0.989	0.986	0.984	0.989
	mR	0.995	0.996	0.998	**0.998**	0.992	0.995	0.979	0.990
	mF1	0.995	0.996	0.998	**0.999**	0.990	0.991	0.982	0.990
	mACC (%)	99.97	99.98	99.84	**99.87**	99.10	99.12	98.24	99.04
	AUC (%)	99.84	99.83	99.92	**99.98**	99.47	99.18	98.25	99.86
Fold 3	mP	0.992	0.993	0.996	**0.997**	0.983	0.977	0.980	0.989
	mR	0.995	0.996	0.997	**1.00**	0.989	0.992	0.982	0.990
	mF1	0.994	0.994	0.997	**0.997**	0.986	0.984	0.981	0.990
	mACC (%)	99.38	99.41	99.71	**99.73**	98.62	98.45	98.11	98.64
	AUC (%)	99.84	99.80	**99.92**	99.90	99.12	98.63	98.11	99.64
Fold 4	mP	0.994	0.996	0.998	**0.999**	0.988	0.984	0.983	0.989
	mR	0.992	0.993	0.999	**0.999**	0.991	0.994	0.982	0.991
	mF1	0.993	0.994	0.998	**0.999**	0.990	0.989	0.983	0.990
	mACC (%)	99.36	99.43	99.86	**99.90**	98.96	98.87	98.26	99.00
	AUC (%)	99.92	99.94	**99.99**	99.95	99.26	98.92	98.26	99.82
Fold 5	mP	0.987	0.988	0.997	**0.999**	0.987	0.982	0.982	0.986
	mR	0.993	0.993	0.997	**0.998**	0.990	0.992	0.980	0.989
	mF1	0.990	0.991	0.997	**0.998**	0.989	0.987	0.981	0.987
	mACC (%)	99.08	99.06	99.77	**99.83**	98.95	98.81	98.18	98.81
	AUC (%)	99.69	99.74	99.96	**99.96**	99.25	98.88	98.18	99.77

*Bold values indicate best results.

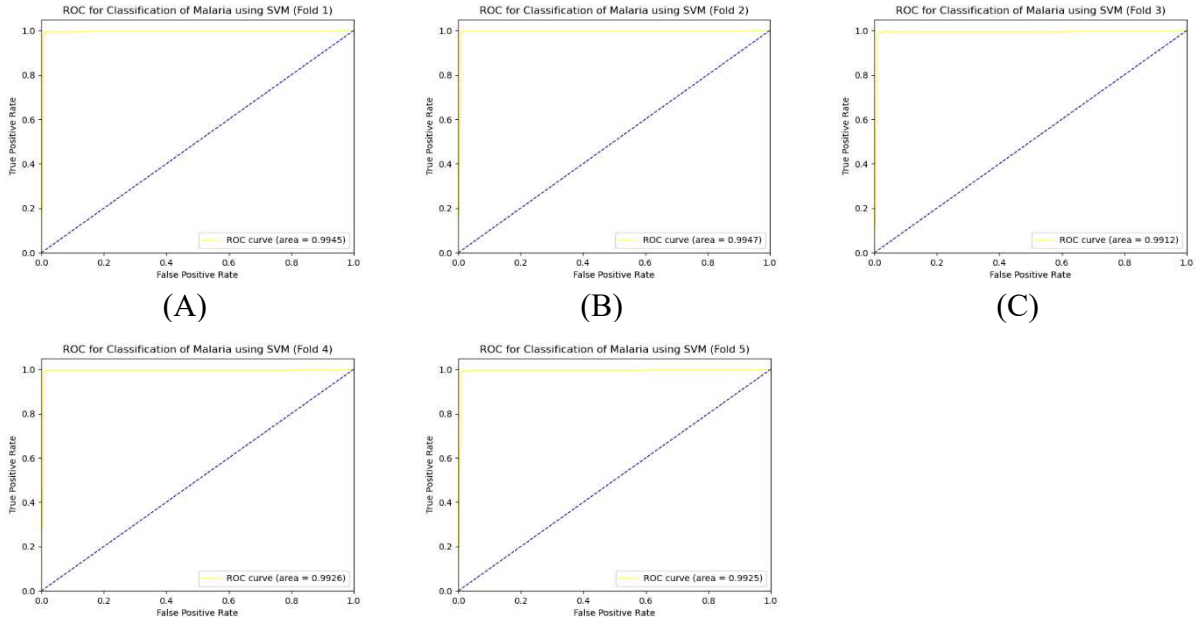

(A) (B) (C)

(D) (E)

Figure 20. ROCs on LPDCNN-SVM (A) fold 1, (B) fold 2, (C) fold 3, (D) fold 4, and (E) fold 5.

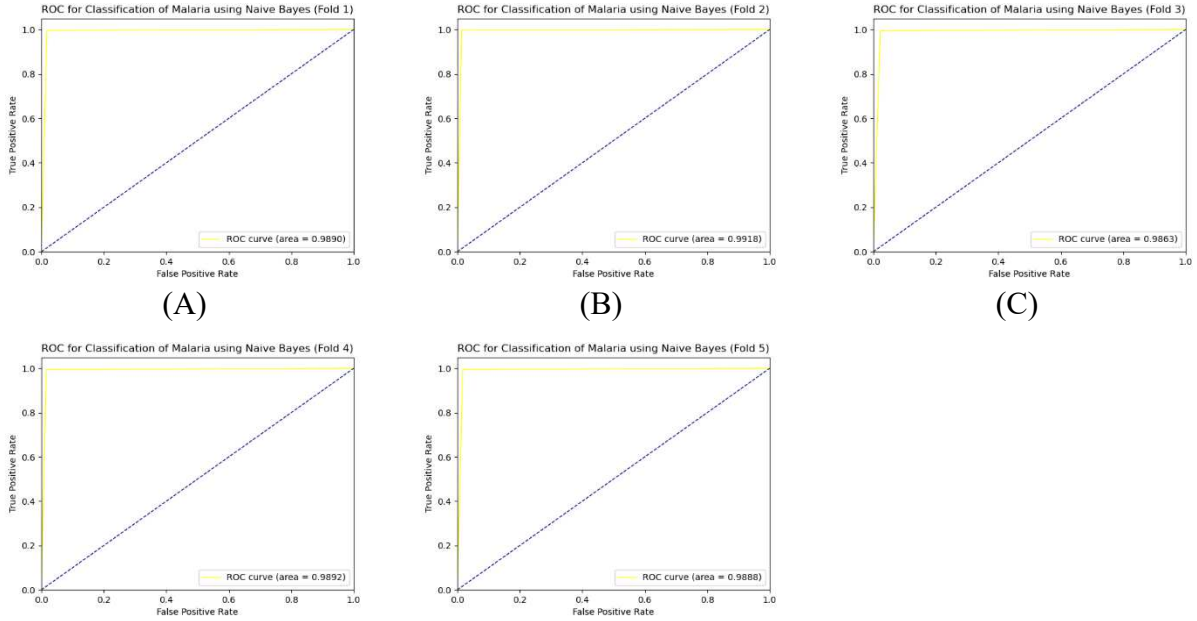

Figure 21. ROCs on LPDCNN-GNB (A) fold 1, (B) fold 2, (C) fold 3, (D) fold 4, and (E) fold 5.

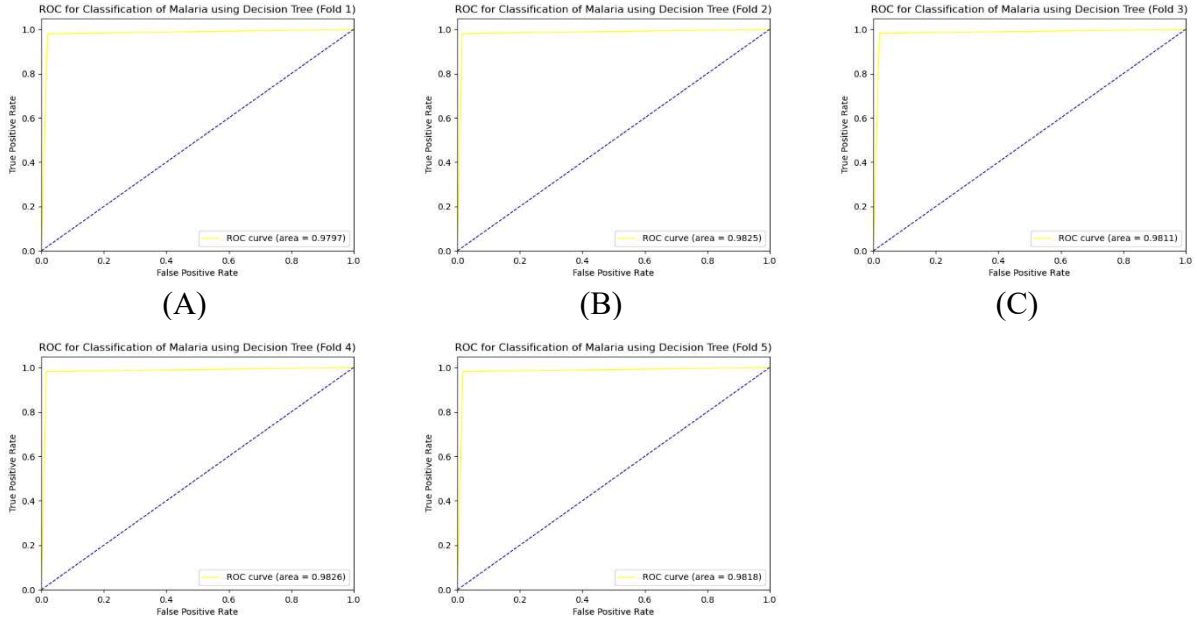

Figure 22. ROCs on LPDCNN-DT (A) fold 1, (B) fold 2, (C) fold 3, (D) fold 4, and (E) fold 5.

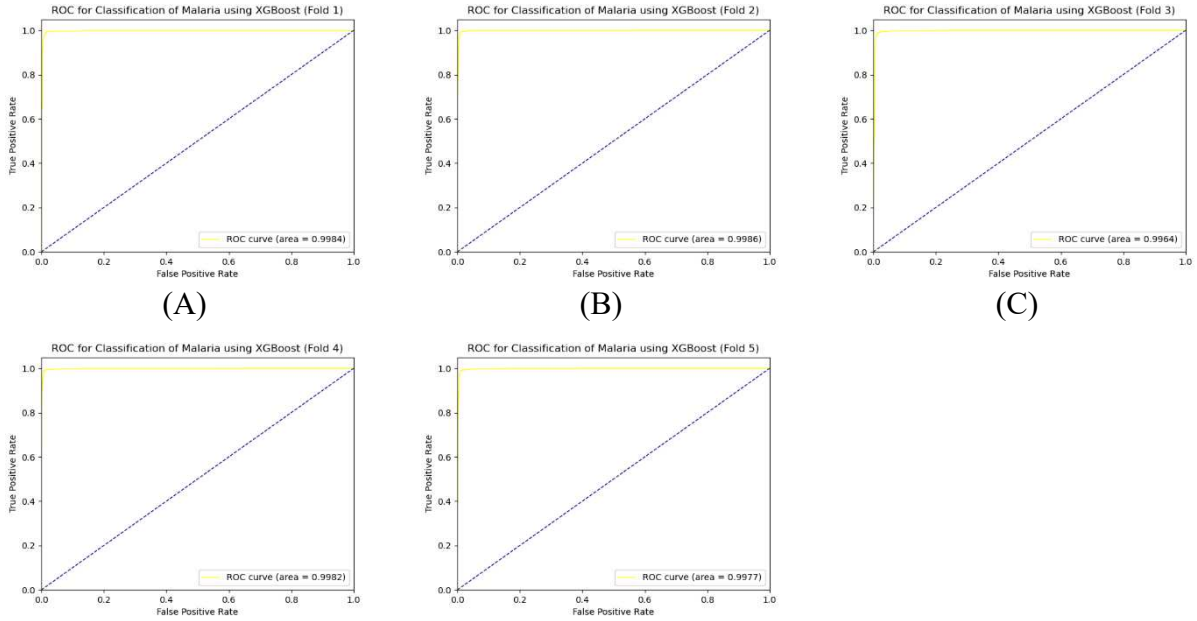

Figure 23. ROCs on LPDCNN-XGBoost (A) fold 1, (B) fold 2, (C) fold 3, (D) fold 4, and (E) fold 5.

3.4 Computational time comparisons

Table 6 compares PNCNN and LPDCNN with ELM, RELM, and other well-known ML models regarding computational time, including training and testing for each CV. Our LPDCNN-RELM model is unique and significant as it requires considerably less time for training and testing than previous SOTA models comparatively. Our proposed system is more reliable as it took only less 0.1346 seconds for training and 0.00249 seconds for testing to generate the result. LPDCNN-GNB required less training time, although testing took longer than LPDCNN-RELM. This model's training time is long (2.1892 seconds), but the testing time is efficient, utilizing DT due to less time. Although SVM showed comparatively better performance scores, this technique may not be efficient for real-time analysis due to high computational time requirements (23.834 seconds for training and 3.6006 seconds for testing). For real-time analysis of many RBC segmented samples, LPDCNN-RELM stands out as superior as it strikes a better balance between analytical efficiency and accuracy. The timing visualization is presented at Figure 24.

Table 6. Comparative computational time requirements on PNCNN, LPDCNN and other SOTA models with TELM and RELM for each CV.

CV		PNCNN +TELM	PNCNN +RELM	LPDCNN +TELM	LPDCNN +RELM	LPDCNN +SVM	LPDCNN +GNB	LPDCNN +DT	LPDCNN +XGBoost
Fold 1	Training Time (s)	0.5256	0.1396	0.5679	0.1346	22.976	**0.0200**	1.8491	3.0698
	Testing Time (s)	0.00259	0.00260	**0.00249**	0.00269	0.3810	0.0130	0.0029	0.0030
Fold	Training Time (s)	0.4907	0.1336	0.5565	0.1376	21.439	**0.0199**	2.0649	4.5947

	Testing Time (s)	0.00239	0.00259	0.00269	0.00249	3.6006	0.0120	**0.0010**	0.0050
Fold 3	Training Time (s)	0.5106	0.1336	0.5236	0.1386	23.834	**0.0199**	2.2829	4.6135
	Testing Time (s)	0.00260	0.00249	0.00270	0.00259	3.4029	0.0130	**0.0010**	0.0040
Fold 4	Training Time (s)	0.5126	0.1336	0.5075	0.1356	22.557	**0.0199**	2.1892	4.6705
	Testing Time (s)	0.00259	0.00279	0.00274	0.00249	3.5784	0.0110	**0.0010**	0.0040
Fold 5	Training Time (s)	0.4997	0.1376	0.5116	0.1416	22.154	**0.0199**	1.9359	4.5039
	Testing Time (s)	0.00259	0.00259	0.00250	0.00250	3.6061	0.0130	**0.0010**	0.0050

*Bold values indicate best results.

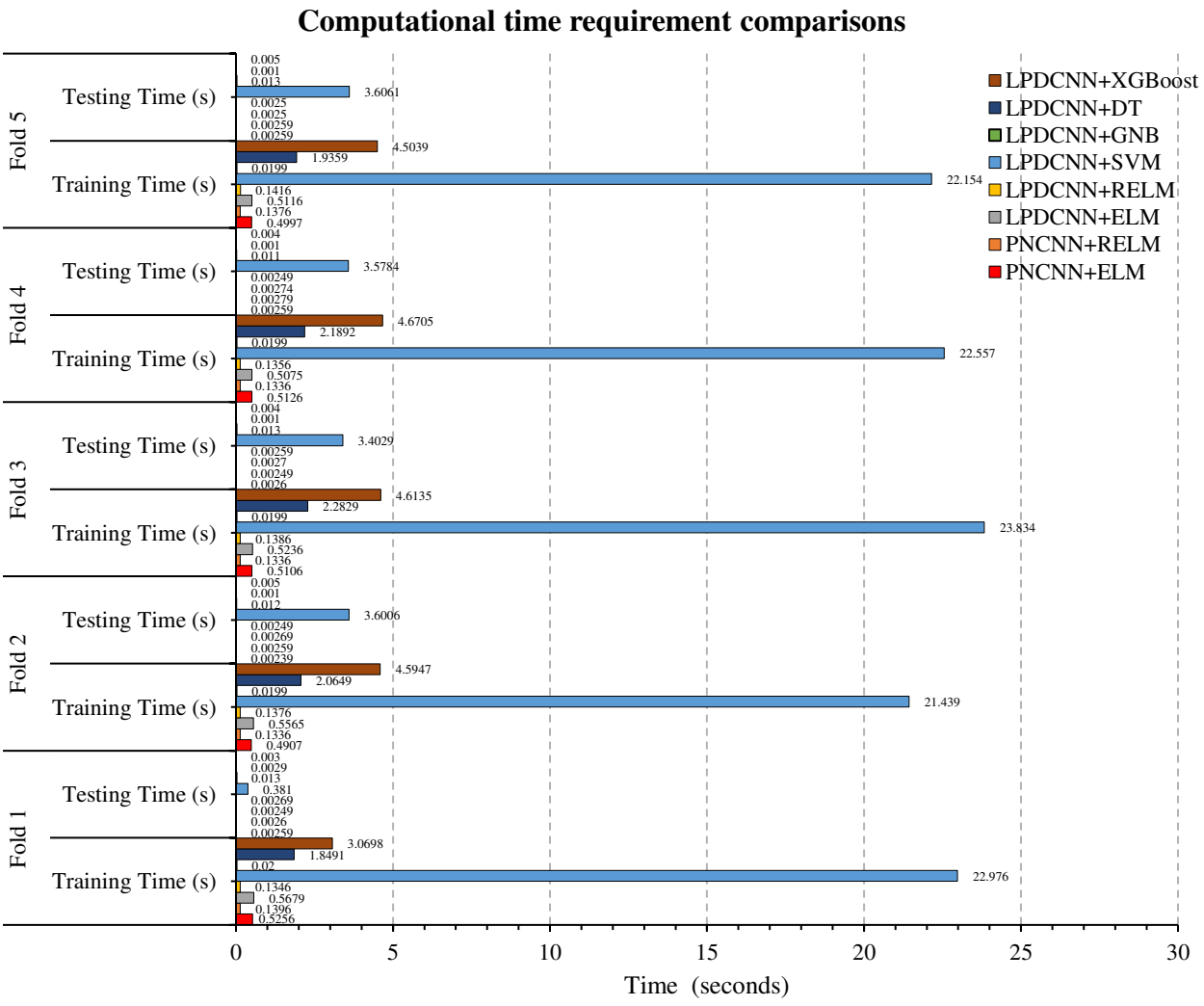

Figure 24. Computational time comparison among the proposed LPDCNN-RELM and other models.

3.5 Computational resource comparisons

Table 7 compares the computational resources of LPDCNN and PNCNN models based on their parameters, layers, and sizes. The LPDCNN-RELM model outperformed all other models with the highest classification accuracy, making it the most successful model. Figure 25 provides a clear visualization of the comprehensive criteria values. The study's results demonstrate that the LPDCNN-RELM approach is dependable and can accurately discriminate between different models. Out of all the malaria dataset models analyzed, the PNCNN model has the most number of parameters 19.56, and a size of 23 MB. The LPDSCNN model is highly efficient in loading and processing due to its compact size of 4.4 MB, 0.362 parameters and 9 CL. This model has only 0.362 million parameters, approximately 53.59 times smaller than the PNCNN model, which has 19.56 million. Despite having fewer layers and smaller sizes, the LPDCNN model can still precisely detect malaria-infected cells (from result section) while using fewer resources. The LPDCNN-RELM model is an exceptional approach that delivers high performance while maintaining a small and resource-efficient design, making it suitable for various applications.

Table 7. Computational resources comparison for classifications.

Performance Criteria	PNCNN	LPDCNN
Total Parameters (Million)	19.56	**0.362**
Trainable Parameters (Million)	19.54	**0.36**
Number of Layers (CL)	**8**	**8**
Size (Megabytes)	23	**4.4**
Average training time (RELM)	**0.1356**	0.1376
Average testing time (RELM)	0.00261	**0.00255**

*Bold values indicate best results.

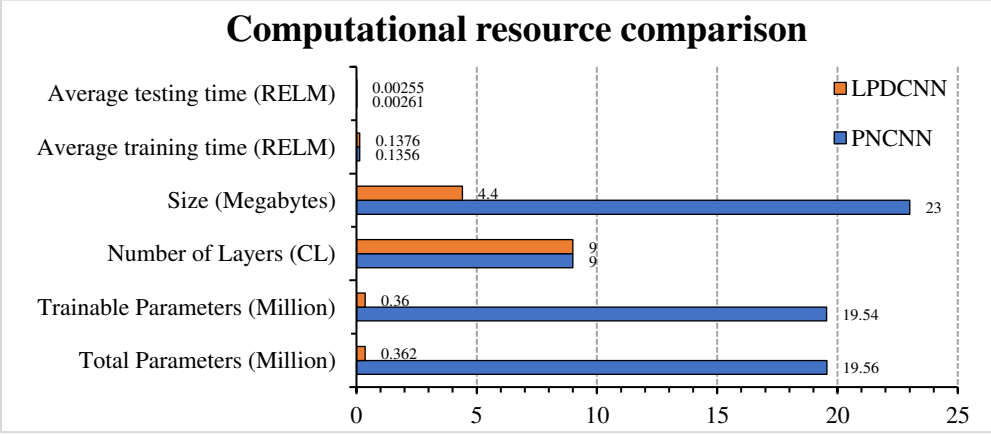

Figure 25. Computational resource comparison between the proposed LPDCNN and PNCNN models.

3.6 Comparative performance analysis of LPDCNN-RELM and SOTA approaches

Table 8 compares the LPDCNN-RELM and SOTA models regarding classification outcomes and computational complexities. Our proposed model for malaria classification surpasses existing techniques in multiple aspects, including precision, recall, f1-score, accuracy, and AUC. We conducted a CV with five evaluations and obtained the average results for each assessment, confirming our approach's reliability.

Goni et al. [24] achieved highly competitive results in precision, recall, f1 score, accuracy, and AUC, with respective values of 99.78%, 99.55%, 99.67%, 99.66%, and 99.96%. However, our proposed LPDCNN-RELM surpassed those scores with improvements of 0.08%, 0.33%, 0.17%, and 0.19% while maintaining a similar AUC score of 99.96%. Additionally, our model has 21.70 times fewer parameters than a DELM (double hidden layer extreme learning machine), demonstrating the superiority of RELM. Khan et al. [25] present aggregated approaches in which multiple ML classifications were applied to processed images. However, their precision was subpar, 82%, and their recall score was 86%. On a comparable set, our LPDCNN-RELM performs noticeably better. According to Fuhad et al. [26], using CNN-SVM and KNN improved classification performance to 99.52% and 99.23%, respectively. However, the computational complexity of these models exceeds that of our LPDCNN method. Islam et al. [27] achieved a remarkable precision of 99.40%, but our proposed framework outperformed it with an AUC of 99.96% and an accuracy of 99.41%. The lightweight nature of our model resulted in improvements of 0.44% and 0.85%, respectively. Figure 26 shows the performance scores of our PNCNN and LPDCNN with TELM and RELM architecture, with LPDCNN-RELM achieving the best score for malaria classification. Additionally, our model has a low parameter count and can process in real time on low-configured devices.

Table 8. Performances comparison different models.

Reference	Models	Classes	Parameters (million)	Precision (%)	Recall (%)	F1 score (%)	Accuracy (%)	AUC (%)
Islam et al. [27]	Transformer	2	-	96.99	95.90	96.44	99.41	99.11
Zhu et al. [41]	ROENet	2		94.79	-	95.69	95.73	-
Goni et al. [24]	CNN-DELM	2	11.5	99.78	99.55	99.67	99.66	99.96
Fuhad et al. [26]	CNN-SVM-KNN	2	-	98.92	99.52	-	99.23	-
Montalbo et al. [42]	Fine-tuned CNN	2	-	93.87	95.46	-	94.70	-
Khan et al. [25]	RF classifier	2	-	82.00	86.00	-	-	-
Efaz et al. [43]	CNN-VGG19-Resnet50	2	-	94.40	96.70	-	95.60	-
Hasan et al. [44]	Traditional ML	2	-	94.65	-	-	91.00	95.00
Fatima et al. [45]	Adaptive learning	2	-	94.66	-	91.80	-	-
Proposed	**LPDCNN-RELM**	**2**	**0.53**	**99.86**	**99.88**	**99.84**	**99.85**	**99.96**

*Bold values indicate best results

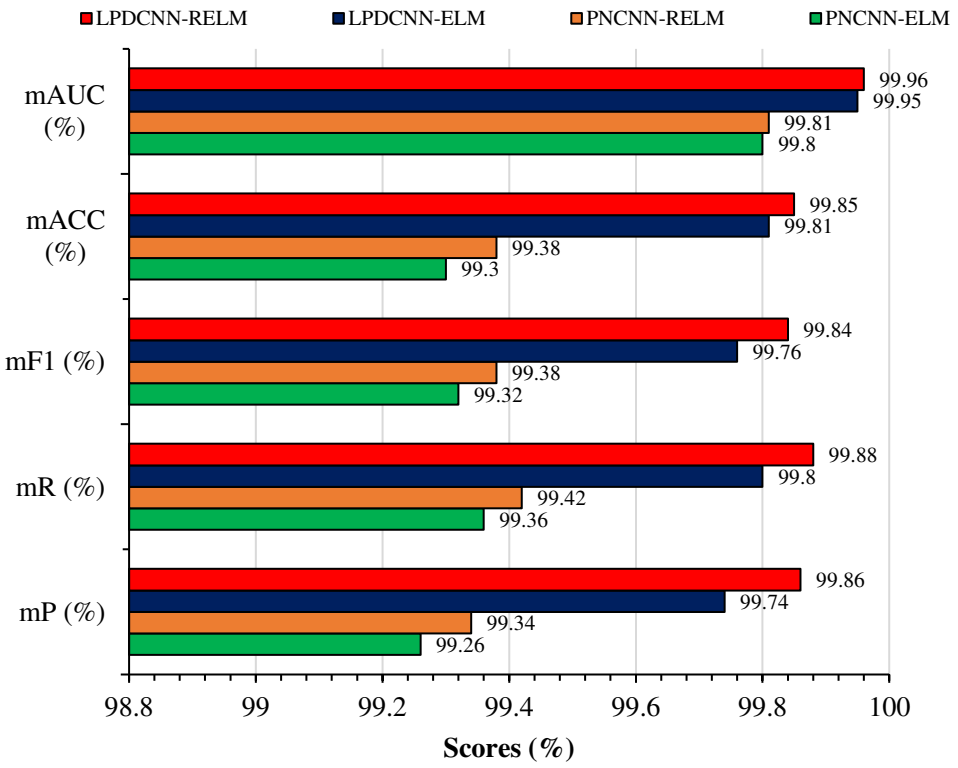

Figure 26. Performance comparison on PNCNN and LPDCNN with ELM and RELM models.

4. Interpretability LPDCNN-RELM using SHAP

The concept of explainable artificial intelligence (XAI) has introduced a transformative paradigm in deep learning, enabling the exploration and understanding of intricate neural networks [46]**.** A noteworthy investigation utilized the SHAP technique to elucidate the decision-making process of the LPDCNN-RELM model in classifying MP. This research utilized the SHAP methodology to offer medical professionals' in-depth insights and explanations, facilitating the practical integration of findings into real-world contexts.

The significance of SHAP is substantial, as it assesses the weight of individual features within the model and quantifies their contributions through rigorous calculations. The study demonstrated the importance of assigning scores to individual pixels in accurately categorizing predicted images. Shapley values were methodically generated by considering all potential combinations of malaria traits, leading to pixelated representations [47]**.** The findings revealed a notable pattern, wherein red pixels demonstrated a significant role in effectively detecting Infected or uninfected malaria cells. On the other hand, the existence of blue pixels suggested the possibility of far away from this class.

Figure 27 depicts the SHAP results, which provided medical experts with a valuable array of explanation images for various classifications, including infected and uninfected cases. It is worth noticing that the SHAP explanation graphics' faint grey backgrounds are integrated with the original input images. In the first row, for instance, red pixels in the SHAP explanation image showed the presence of an uninfected cell. On the other hand, the absence of blue pixels

conclusively ruled out other class categories, such as diseased. Surprisingly, the second row revealed a contrary pattern, with red pixels in the SHAP explanation images indicating the infected class. On the other hand, an abundance of red pixels in the SHAP image precisely recognized the image as belonging to the infected class. In the third row, the concentration of red pixels accurately represented the infected cohort. The presence of blue pixels in the SHAP of other classes, on the other hand, confirmed the lack of malaria. Similarly, the absence of red pixels in the fourth row of the SHAP image provided significant evidence for the absence of MP. These visual SHAP explanations verified the model's findings, giving doctors a deeper understanding of the various strains of malaria detection.

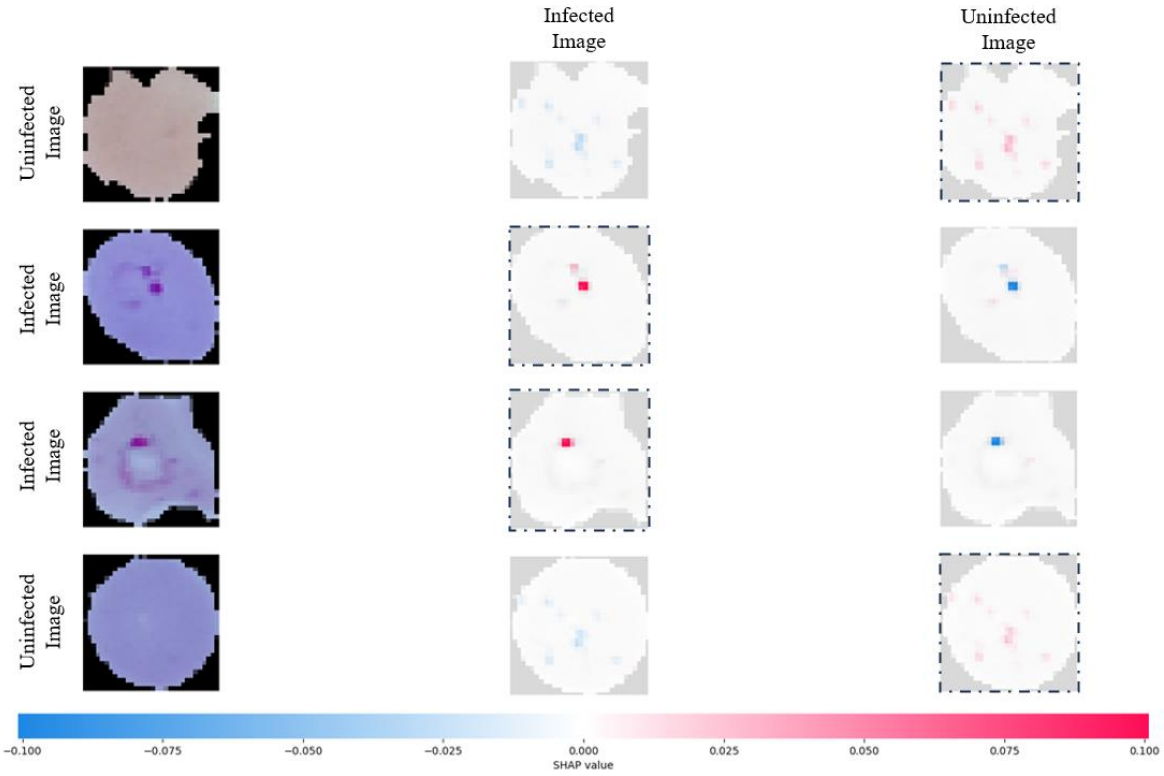

Figure 27. The sample images and the corresponding SHAP explanation images for LPDCNN-RELM.

5. Conclusion

In conclusion, the presented research introduces a novel method for accurately classifying malaria from RBC-segmented images using a combination of LPDCNN and RELM models. Improving the appearance and clarity of essential features while reducing unwanted noise is made possible by incorporating a significant image preprocessing approach called CLAHE and dilation procedures. With only 0.36 million parameters and 8 layers, the proposed LPDCNN architecture effectively collects infected-specific patterns with low computational overhead. The addition of the hybrid ridge regression ELM model, which replaces pseudoinverse with ridge regression, considerably improves classification performance. This innovative method achieves remarkable accuracy values of 99.85±0.071% for binary classifications using five-fold cross-validation.

The LPDCNN-RELM model is exceptionally reliable in recognizing malaria cases, as evidenced by precision, recall, and f1-scores values of 99.86±0.08%, 99.88±0.084%, and 99.84±0.089% with excellent AUC score 99.96±0.037%, respectively. Compared to TELM approaches, the LPDCNN-RELM model is significantly superior by almost 0.20% approximately. This significant improvement in accuracy highlights its promise as a trustworthy instrument for simultaneously identifying diverse patients. Furthermore, the model's minimal computing resource needs allow for seamless implementation on low-powered devices, enhancing its accessibility and practicality in real-world healthcare settings. Medical doctors and hematologists can benefit significantly from SHAP's incorporation because it enables a trustworthy interpretation of the model's outcomes. SHAP's openness and interpretability boost confidence in the categorization results, leading to better decisions and more targeted therapies.
In summary, the proposed LPDCNN-RELM method substantially improves the classification accuracy of malaria and is simple to implement and interpret. This study shows much assurance in finding malaria cases early and treating them successfully, which will improve patient outcomes and save lives.

Author Contribution: Md. Faysal Ahamed and Md. Nahiduzzaman; Conceptualization, Md. Faysal Ahamed and Md. Nahiduzzaman; methodology, Md. Faysal Ahamed, Md. Nahiduzzaman, Mohamed Arselene Ayari, Amith Khandakar, S. M. Riazul Islam; validation, Md. Faysal Ahamed, Md. Nahiduzzaman, Amith Khandakar, and S. M. Riazul Islam; formal analysis, Md. Faysal Ahamed, Md. Nahiduzzaman, and S. M. Riazul Islam; investigation, Mohamed Arselene Ayari and Amith Khandakar; resources, Mohamed Arselene Ayari, Amith Khandakar, and S. M. Riazul Islam; data curation, Md. Nahiduzzaman; writing—original draft, Md. Faysal Ahamed and Md. Nahiduzzaman; writing—review and editing, Mohamed Arselene Ayari, Amith Khandakar, and S. M. Riazul Islam; visualization, Mohamed Arselene Ayari, Amith Khandakar, S. M. Riazul Islam; supervision, Mohamed Arselene Ayari, Amith Khandakar, and S. M. Riazul Islam; project administration, Mohamed Arselene Ayari, Amith Khandakar, S. M. Riazul Islam; funding acquisition, Mohamed Arselene Ayari, Amith Khandakar, and S. M. Riazul Islam; All authors have read and agreed to the published version of the manuscript.

Funding' section: No funding was obtained for this study.

Data Availability: Data will be made available on request.

Conflict of Interest: There are no relevant financial or non-financial competing interests to report.

6. References

[1] W.H. Organization, Malaria microscopy quality assurance manual, version 2, World Health Organization, 2016.

[2] D. Srivastava, S. Muhuri, S.S. Singh, M. Verma, An Extensive Survey on Classification of Malaria Parasites in Patients Based on Fuzzy Approaches, in: T. Som, O. Castillo, A.K. Tiwari, S. Shreevastava (Eds.), Fuzzy, Rough Intuitionistic Fuzzy Set Approaches Data Handl. Theory Appl., Springer Nature Singapore, Singapore, 2023: pp. 87–100. https://doi.org/10.1007/978-981-19-8566-9_5.

[3] W.R.J. Taylor, J. Hanson, G.D.H. Turner, N.J. White, A.M. Dondorp, Respiratory manifestations

of malaria, Chest. 142 (2012) 492–505.

[4] W.H. Wernsdorfer, The development and spread of drug-resistant malaria, Parasitol. Today. 7 (1991) 297–303. https://doi.org/10.1016/0169-4758(91)90262-M.

[5] A.F. Cowman, B.S. Crabb, Invasion of red blood cells by malaria parasites, Cell. 124 (2006) 755–766. https://doi.org/10.1016/j.cell.2006.02.006.

[6] M. Singh, K. Saha, S. Chand, L.S.-A. tropica, undefined 2019, The economic cost of malaria at the household level in high and low transmission areas of central India, Elsevier. (n.d.). https://www.sciencedirect.com/science/article/pii/S0001706X18311379 (accessed July 23, 2023).

[7] Y.G. Gezahegn, Y.H.G. Medhin, E.A. Etsub, G.N.G. Tekele, Malaria Detection and Classification Using Machine Learning Algorithms, in: F. Mekuria, E.E. Nigussie, W. Dargie, M. Edward, T. Tegegne (Eds.), Inf. Commun. Technol. Dev. Africa, Springer International Publishing, Cham, 2018: pp. 24–33.

[8] S.K. Mondal, M. Islam, M.O. Faruque, M.S. Turja, M.S.U. Yusuf, Efficient Malaria Cell Image Classification Using Deep Convolutional Neural Network, in: M. Ahmad, M.S. Uddin, Y.M. Jang (Eds.), Proc. Int. Conf. Inf. Commun. Technol. Dev., Springer Nature Singapore, Singapore, 2023: pp. 435–445.

[9] P.M. Neelamraju, B.S. Penugonda, A. Koganti, A. Unnam, K. Tiwari, Voting Based Classification System for Malaria Parasite Detection, in: H. Sharma, A.K. Saha, M. Prasad (Eds.), Proc. Int. Conf. Intell. Vis. Comput. (ICIVC 2022), Springer Nature Switzerland, Cham, 2023: pp. 338–347.

[10] D. Agarwal, K. Sashanka, S. Madan, A. Kumar, P. Nagrath, R. Jain, Malaria Cell Image Classification Using Convolutional Neural Networks (CNNs), in: D. Gupta, Z. Polkowski, A. Khanna, S. Bhattacharyya, O. Castillo (Eds.), Proc. Data Anal. Manag., Springer Singapore, Singapore, 2022: pp. 21–36.

[11] A.H. Alharbi, C. V. Aravinda, J. Shetty, M.Y. Jabarulla, K.B. Sudeepa, S.K. Singh, Computational Models-Based Detection of Peripheral Malarial Parasites in Blood Smears, Contrast Media Mol. Imaging. 2022 (2022). https://doi.org/10.1155/2022/9171343.

[12] D.K. Das, M. Ghosh, M. Pal, A.K. Maiti, C. Chakraborty, Machine learning approach for automated screening of malaria parasite using light microscopic images, Micron. 45 (2013) 97–106. https://doi.org/10.1016/j.micron.2012.11.002.

[13] L. Yunda, A. Alarcón, J. Millán, Automated Image Analysis Method for p-vivax Malaria Parasite Detection in Thick Film Blood Images, Sist. y Telemática. 10 (2012) 9. https://doi.org/10.18046/syt.v10i20.1151.

[14] I.K.E. Purnama, F.Z. Rahmanti, M.H. Purnomo, Malaria parasite identification on thick blood film using genetic programming, Proc. 2013 3rd Int. Conf. Instrumentation, Commun. Inf. Technol., Biomed. Eng. Sci. Technol. Improv. Heal. Safety, Environ., ICICI-BME 2013. (2013) 194–198. https://doi.org/10.1109/ICICI-BME.2013.6698491.

[15] L. Rosado, J.M.C. Da Costa, D. Elias, J.S. Cardoso, Automated Detection of Malaria Parasites on Thick Blood Smears via Mobile Devices, Procedia Comput. Sci. 90 (2016) 138–144. https://doi.org/10.1016/j.procs.2016.07.024.

[16] D. Bibin, M.S. Nair, P. Punitha, Malaria Parasite Detection From Peripheral Blood Smear Images Using Deep Belief Networks, IEEE Access. 5 (2017) 9099–9108.

[17] S. Rajaraman, S.K. Antani, M. Poostchi, K. Silamut, M.A. Hossain, R.J. Maude, S. Jaeger, G.R.

Thoma, Pre-trained convolutional neural networks as feature extractors toward improved malaria parasite detection in thin blood smear images., PeerJ. 6 (2018) e4568. https://doi.org/10.7717/peerj.4568.

[18] K. Sriporn, C.-F. Tsai, C.-E. Tsai, P. Wang, Analyzing Malaria Disease Using Effective Deep Learning Approach, Diagnostics. 10 (2020). https://doi.org/10.3390/diagnostics10100744.

[19] F. Chollet, Xception: Deep learning with depthwise separable convolutions, in: Proc. IEEE Conf. Comput. Vis. Pattern Recognit., Institute of Electrical and Electronics Engineers Inc., 2017: pp. 1251–1258. https://doi.org/10.1109/CVPR.2017.195.

[20] C. Wang, D. Chen, L. Hao, X. Liu, Y. Zeng, J. Chen, G. Zhang, Pulmonary image classification based on inception-v3 transfer learning model, IEEE Access. 7 (2019) 146533–146541.

[21] L. Wen, X. Li, L. Gao, A transfer convolutional neural network for fault diagnosis based on ResNet-50, Neural Comput. Appl. 32 (2020) 6111–6124.

[22] S. Tammina, Transfer learning using vgg-16 with deep convolutional neural network for classifying images, Int. J. Sci. Res. Publ. 9 (2019) 143–150.

[23] F.N. Iandola, S. Han, M.W. Moskewicz, K. Ashraf, W.J. Dally, K. Keutzer, SqueezeNet: AlexNet-level accuracy with 50x fewer parameters and< 0.5 MB model size, ArXiv Prepr. ArXiv1602.07360. (2016).

[24] M.O.F. Goni, M.N.I. Mondal, S.M. Riazul Islam, M. Nahiduzzaman, M. Robiul Islam, M.S. Anower, K.S. Kwak, Diagnosis of Malaria Using Double Hidden Layer Extreme Learning Machine Algorithm With CNN Feature Extraction and Parasite Inflator, IEEE Access. 11 (2023) 4117–4130. https://doi.org/10.1109/ACCESS.2023.3234279.

[25] A. Khan, K. Gupta, … D.V.-2020 I.J., undefined 2020, Cidmp: Completely interpretable detection of malaria parasite in red blood cells using lower-dimensional feature space, Ieeexplore.Ieee.OrgA Khan, KD Gupta, D Venugopal, N Kumar2020 Int. Jt. Conf. Neural Networks (IJCNN), 2020•ieeexplore.Ieee.Org. (2020). https://ieeexplore.ieee.org/abstract/document/9206885/ (accessed July 22, 2023).

[26] K.M.F. Fuhad, J.F. Tuba, M.R.A. Sarker, S. Momen, N. Mohammed, T. Rahman, Deep Learning Based Automatic Malaria Parasite Detection from Blood Smear and Its Smartphone Based Application, Diagnostics. 10 (2020) 329. https://doi.org/10.3390/DIAGNOSTICS10050329.

[27] M.R. Islam, M. Nahiduzzaman, M.O.F. Goni, A. Sayeed, M.S. Anower, M. Ahsan, J. Haider, Explainable Transformer-Based Deep Learning Model for the Detection of Malaria Parasites from Blood Cell Images, Sensors. 22 (2022) 1–20. https://doi.org/10.3390/s22124358.

[28] I. Mohanty, P.A. Pattanaik, T. Swarnkar, Automatic detection of malaria parasites using unsupervised techniques, in: Proc. Int. Conf. ISMAC Comput. Vis. Bio-Engineering 2018, Springer, 2019: pp. 41–49.

[29] Y. Dong, Z. Jiang, H. Shen, W. David Pan, L.A. Williams, V.V.B. Reddy, W.H. Benjamin, A.W. Bryan, Evaluations of deep convolutional neural networks for automatic identification of malaria infected cells, in: 2017 IEEE EMBS Int. Conf. Biomed. Heal. Informatics, 2017: pp. 101–104. https://doi.org/10.1109/BHI.2017.7897215.

[30] D. Anggraini, A.S. Nugroho, C. Pratama, I.E. Rozi, Aulia Arif Iskandar, Reggio Nurtanio Hartono, Automated status identification of microscopic images obtained from malaria thin blood smears, Proc. 2011 Int. Conf. Electr. Eng. Informatics. (2011). https://doi.org/10.1109/ICEEI.2011.6021762.

[31] S. Kaewkamnerd, C. Uthaipibull, A. Intarapanich, M. Pannarut, S. Chaotheing, S. Tongsima, An automatic device for detection and classification of malaria parasite species in thick blood film, BMC Bioinformatics. 13 (2012) S18. https://doi.org/10.1186/1471-2105-13-S17-S18.

[32] S. Chatterjee, P. Majumder, Automated Classification and Detection of Malaria Cell Using Computer Vision, in: D. Bhattacharjee, D.K. Kole, N. Dey, S. Basu, D. Plewczynski (Eds.), Proc. Int. Conf. Front. Comput. Syst., Springer Singapore, Singapore, 2021: pp. 473–482.

[33] D.H.J. Thijssen, M.A. Black, K.E. Pyke, J. Padilla, G. Atkinson, R.A. Harris, B. Parker, M.E. Widlansky, M.E. Tschakovsky, D.J. Green, Assessment of flow-mediated dilation in humans: A methodological and physiological guideline, Am. J. Physiol. - Hear. Circ. Physiol. 300 (2011) 2–12. https://doi.org/10.1152/AJPHEART.00471.2010/ASSET/IMAGES/LARGE/ZH40011196500005.JPEG.

[34] A.W. Setiawan, T.R. Mengko, O.S. Santoso, A.B. Suksmono, Color retinal image enhancement using CLAHE, Proc. - Int. Conf. ICT Smart Soc. 2013 "Think Ecosyst. Act Converg. ICISS 2013. (2013) 215–217. https://doi.org/10.1109/ICTSS.2013.6588092.

[35] S. Santurkar, D. Tsipras, A. Ilyas, A. M\kadry, How Does Batch Normalization Help Optimization?, in: Proc. 32nd Int. Conf. Neural Inf. Process. Syst., Curran Associates Inc., Red Hook, NY, USA, 2018: pp. 2488–2498.

[36] S. Wen, S. Xiao, Y. Yang, Z. Yan, Z. Zeng, T. Huang, Adjusting Learning Rate of Memristor-Based Multilayer Neural Networks via Fuzzy Method, IEEE Trans. Comput. Des. Integr. Circuits Syst. 38 (2019) 1084–1094. https://doi.org/10.1109/TCAD.2018.2834436.

[37] G.-B. Huang, Q.-Y. Zhu, C.-K. Siew, Extreme learning machine: Theory and applications, Neurocomputing. 70 (2006) 489–501. https://doi.org/https://doi.org/10.1016/j.neucom.2005.12.126.

[38] M. Nahiduzzaman, M.O.F. Goni, R. Hassan, M.R. Islam, M.K. Syfullah, S.M. Shahriar, M.S. Anower, M. Ahsan, J. Haider, M. Kowalski, Parallel CNN-ELM: A multiclass classification of chest X-ray images to identify seventeen lung diseases including COVID-19., Expert Syst. Appl. 229 (2023) 120528. https://doi.org/10.1016/j.eswa.2023.120528.

[39] D.M.W. Powers, Evaluation: from precision, recall and F-measure to ROC, informedness, markedness and correlation, ArXiv. abs/2010.1 (2011).

[40] B.N. Chaithanya, T.J. Swasthika Jain, A. Usha Ruby, A. Parveen, An approach to categorize chest X-ray images using sparse categorical cross entropy, Indones. J. Electr. Eng. Comput. Sci. (2021) 1700–1710.

[41] Z. Zhu, S. Wang, Y. Zhang, ROENet: A ResNet-Based Output Ensemble for Malaria Parasite Classification, Electron. 11 (2022). https://doi.org/10.3390/electronics11132040.

[42] F. Montalbo, A.A.-K.T. on I. and, undefined 2021, Empirical analysis of a fine-tuned deep convolutional model in classifying and detecting malaria parasites from blood smears, Acad. Montalbo, AS AlonKSII Trans. Internet Inf. Syst. 2021•academia.Edu. (n.d.). https://www.academia.edu/download/84150435/TIIS_20Vol_2015__20No_201-9.pdf (accessed July 22, 2023).

[43] E.T. Efaz, F. Alam, M.S. Kamal, Deep cnn-supported ensemble cadx architecture to diagnose malaria by medical image, Adv. Intell. Syst. Comput. 1309 (2021) 231–243. https://doi.org/10.1007/978-981-33-4673-4_20.

[44] M. Hasan, S. Islam, A. Dey, A. Das, S.T.-I.C. on, undefined 2021, Detection of malaria disease using image processing and machine learning, SpringerMM Hasan, S Islam. A Dey, A Das, SC TistaInternational Conf. Intell. Comput. Optim. 2021•Springer. 371 (2022) 457–466. https://doi.org/10.1007/978-3-030-93247-3_45.

[45] T. Fatima, M.S. Farid, Automatic detection of Plasmodium parasites from microscopic blood images, J. Parasit. Dis. 44 (2020) 69–78. https://doi.org/10.1007/s12639-019-01163-x.

[46] X. Peng, Y. Li, I.W. Tsang, H. Zhu, J. Lv, J.T. Zhou, XAI beyond Classification: Interpretable Neural Clustering, J. Mach. Learn. Res. 23 (2022).

[47] M. Bhandari, T.B. Shahi, B. Siku, A. Neupane, Explanatory Classification of CXR Images into COVID-19, Pneumonia and Tuberculosis Using Deep Learning and XAI, Comput. Biol. Med. 150 (2022). https://doi.org/10.1016/j.compbiomed.2022.106156.